ABSORPTION LOSSES IN EPITAXIAL PbTe FILMS FOR POTENTIAL INTEGRATED OPTICS APPLICATION

W. H. Weber, et al

Ford Motor Company

Prepared for:

Naval Research Laboratory
Advanced Research Projects Agency

February 1974

SECURITY CLASSIFICATION OF THIS PAGE (When Data Entered)

REPORT DOCUMENTATION PAGE

READ INSTRUCTIONS BEFORE COMPLETING FORM

1. REPORT NUMBER

2. GOVT ACCESSION NO.

3. RECIPIENT'S CATALOG NUMBER

4. TITLE (and Subtitle)
Absorption Losses in Epitaxial PbTe Films for Potential Integrated Optics Application

5. TYPE OF REPORT & PERIOD COVERED
Final Technical Report
1 Oct. 1973 - 31 Dec. 1973

6. PERFORMING ORG. REPORT NUMBER

7. AUTHOR(s)
W. H. Weber, S. L. McCarthy, M. Mikkor

8. CONTRACT OR GRANT NUMBER(s)
N00014-73-C-0289

9. PERFORMING ORGANIZATION NAME AND ADDRESS
Scientific Research Staff
Ford Motor Company, P. O. Box 2053
Dearborn, Michigan 48121

10. PROGRAM ELEMENT, PROJECT, TASK AREA & WORK UNIT NUMBERS
ARPA Order No. 2327
Program Code 3010

11. CONTROLLING OFFICE NAME AND ADDRESS
Sponsored by the Advanced Research Projects Agency, Arlington, Virginia 22209

12. REPORT DATE
28 February 1974

13. NUMBER OF PAGES
35

14. MONITORING AGENCY NAME & ADDRESS (if different from Controlling Office)
Naval Research Laboratory
Washington, D. C. 20375

15. SECURITY CLASS. (of this report)
Unclassified

15a. DECLASSIFICATION/DOWNGRADING SCHEDULE

16. DISTRIBUTION STATEMENT (of this Report)
Unlimited

17. DISTRIBUTION STATEMENT (of the abstract entered in Block 20, if different from Report)

18. SUPPLEMENTARY NOTES

19. KEY WORDS (Continue on reverse side if necessary and identify by block number)
Optical Waveguide
Losses in Epitaxial Films
Thin-Film Lasers
Integrated Optics

20. ABSTRACT (Continue on reverse side if necessary and identify by block number) Optical absorption measurements at 300 K and 77K in the 2.5-12 μm range are presented for epitaxial PbTe films grown on BaF_2 substrates. Effects due to carrier concentrations, growth conditions, and possible impurities are discussed. In high carrier concentration films ($p > 10^{18}$ cm^{-3}) the absorption is free-carrier limited, while in low p material the absorption appears to be impurity limited. The impurity limited absorption, which shows wide variations between samples, correlates with the observation of Cl in the ion back-scattering spectra. The lowest observed 10 μm loss is 16 cm^{-1}. A threshold analysis on PbTe diode lasers made with annealed samples indicates the threshold gain is 10-20 cm^{-1}, about a factor of 10 below that obtained in similar lasers in unannealed films.

DD FORM 1 JAN 73 1473 EDITION OF 1 NOV 65 IS OBSOLETE

Unclassified

SECURITY CLASSIFICATION OF THIS PAGE (When Data Entered)

ABSORPTION LOSSES IN EPITAXIAL PbTe FILMS FOR POTENTIAL INTEGRATED OPTICS APPLICATIONS

FINAL TECHNICAL REPORT

February 1974

BY

W. H. Weber*, S. L. McCarthy and M. Mikkor
Scientific Research Staff, Ford Motor Company, Dearborn, Michigan 48121

*Principal Investigator
Phone: (Area 313) 337-6291

Prepared for the Naval Research Laboratory under Contract Number N00014-73-C-0289 - 1 March 1973 to 31 December 1973 --- $98,945.

SPONSORED BY

Advanced Research Projects Agency
ARPA Order No. 2327, Program Code No. 3D10

TABLE OF CONTENTS

ABSORPTION LOSSES IN EPITAXIAL PbTe FILMS FOR POTENTIAL INTEGRATED OPTICS APPLICATIONS

W. H. Weber, S. L. McCarthy and M. Mikkor
Scientific Research Staff, Ford Motor Company, Dearborn, Michigan 48121

SUMMARY

This report covers research on the feasibility of developing an integrated optics heterodyne receiver based on the epitaxial growth of Pb-salt films on BaF_2 substrates. A number of experimental and theoretical results pertinent to propagation losses in PbTe films are discussed. Optical absorption measurements at 300K and 77K in the 2.5-12 μm range are given for PbTe films. Effects due to carrier concentration, growth conditions, and possible impurities are discussed. Films grown on BaF_2 substrates have substantially lower below-bandgap absorption coefficients than those grown on alkali halides. In higher carrier concentration material ($p \geq 10^{18}$ cm^{-3}) the absorption is free carrier limited, while in low carrier concentration material the absorption appears to be impurity limited. The impurity limited absorption, which shows wide variations between samples, correlates with the observation of Cℓ in the ion back-scattering spectra. The lowest observed 10 μm loss is 16 cm^{-1}.

A threshold analysis is done on PbTe lasers made with annealed samples. The analysis yields values of 10-20 cm^{-1} for the optical gain at threshold, about a factor of 10 below the values obtained in similar lasers in unannealed films. A calculation of the losses due to the Pb metal boundary indicates the TE_o mode in a typical film shows roughly 1 cm^{-1} attenuation coefficient, while the TM_o mode shows a loss 40 times larger. This drastic difference is probably the reason these lasers show such a strong preference for TE polarization.

I. INTRODUCTION

Epitaxial PbTe films on BaF_2 have yielded a variety of high quality active devices such as lasers, detectors, and field-effect transistors suitable for applications in integrated optical circuits.[1-4] The use of these films as passive optical waveguides, however, depends upon achieving low loss propagation with an absorption coefficient $\alpha \lesssim 1\ cm^{-1}$. In this report we discuss a number of experimental and theoretical results pertinent to propagation losses in PbTe films. Previous reports discussed the fabrication and characterization of PbTe lasers and grating couplers. This report covers only the work done in the last quarter, with a discussion in the last Section regarding the general feasibility of viable integrated optics systems using the Pb-salt films.

Measurements of the below-bandgap absorption in PbTe films and a discussion of these results are presented in Sections II and III, respectively. Extensive experiments of this type have been reported on bulk Pb-salt materials,[5-8] and two reports have been made on epitaxial Pb-salt films using NaCl substrates.[9,10] The bulk-crystal measurements indicated reasonable agreement at room temperature with the classical Drude expression[11] for calculating the free-carrier absorption. A number of authors[12-15] have also used the formula for estimating the absorption at liquid He temperatures in Pb-salt lasers. The classical expression predicts that absorption coefficients less than $1\ cm^{-1}$ can be easily obtained with carrier concentrations in the middle $10^{16}\ cm^{-3}$ range. However, no absorption coefficients this small have actually been reported in any of the Pb-salts. In addition, several optical absorption and magnetoreflection[7,8]

experiments indicate values of α at low temperatures from 2 to 100 times larger than predicted with the classical formula.

As pointed out by Dumke,[16] a condition for the validity of the classical expression in a degenerate semiconductor is $\hbar\omega < E_f$, where $\hbar\omega$ is the photon energy and E_f the Fermi energy. For most Pb-salts this condition is never satisfied at low termperatures in the infrared. A complete analysis of the losses in these materials requires a quantum mechanical calculation of free carrier absorption in the presence of acoustic phonon, optical phonon, and ionized impurity scattering, with the relative amounts of each mechanism present changing with temperature and carrier concentration. In general we would expect the absorption to be larger than the classical value and to have a wavelength dependence $\alpha \sim \lambda^{1.5-3}$ depending on the dominant scattering mechanism.[17-19]

Our experiments indicate that substantially lower losses result from films on BaF_2 as opposed to alkali halide substrates. The losses, however, are still too large for most waveguiding applications. Previous waveguide experiments[20] with PbTe on BaF_2 indicated a lower limit on α of ≈ 12 cm^{-1} at $\lambda = 10$ μm. The present measurements confirm this result, the lowest observed 10 μm loss value being 16 cm^{-1}. This value appears to be limited at present by impurities introduced in the film growth process.

Estimates of the propagation losses in PbTe films obtained by calculating the approximate threshold gain in unannealed lasers, indicated anomalously large values $\sim 10^2$ cm^{-1} for the absorption coefficient.[4] An improved threshold analysis, which includes the effects of nonuniform current distribution inherent in the thin films, is presented in Section IV. Applying this analysis to our annealed laser films and using a value of 5%

for the internal quantum efficiency yields values for α in the range 10-20 cm^{-1}. These values are comparable to those observed in a number of bulk Pb-salt diode lasers.[12-15]

In the annealed laser samples the injected minority carriers are expected to be nearly uniformly distributed under the Pb contact. The loss from the metal boundary must then be considered in the analysis. In Section V we give a calculation of the losses in a metal covered dielectric waveguide. The TM modes show substantially higher losses than TE modes, which may explain the consistent TE polarization shown by these lasers.

II. EXPERIMENTAL DESCRIPTION

The optical absorption was obtained from an analysis of transmission data taken with a Perkin-Elmer Model 180 grating infrared spectrometer. Measurements were made from 2.5 μm to 12 μm, well below the absorption edge. At longer wavelengths the BaF_2 substrate introduces significant absorption. Two matched sample holders were placed in the specimen and reference chambers. Two dewars with KCℓ windows were used for measurements at liquid nitrogen temperatures. Blank BaF_2 substrates were employed to check transmission accuracy. The resolution of the spectrometer during the run was several wavenumbers, adequate for the multiple interference structure that was observed. The reproducibility of the transmission on several BaF_2 substrates was better than 1%. Repeatability of the spectra on the same sample was better than 0.5%. The PbTe samples were grown on air-cleaved BaF_2 substrates using the techniques developed by Holloway.[3] Figure 1 shows a typical transmission curve. A BaF_2 spectrum is included.

The absorption and index of refraction of the films are determined by noting the positions and the absolute transmission values of the interference peaks. For low loss films the index of refraction can be obtained from the expression[21]

$$n = \frac{m}{2}\frac{\lambda}{d} \qquad (1)$$

where λ is the wavelength at peak maxima, d is the thickness of the PbTe film obtained interferometrically and m is the fringe index number. The major source of error in determining the index is the uncertainty (± 0.1 μm)

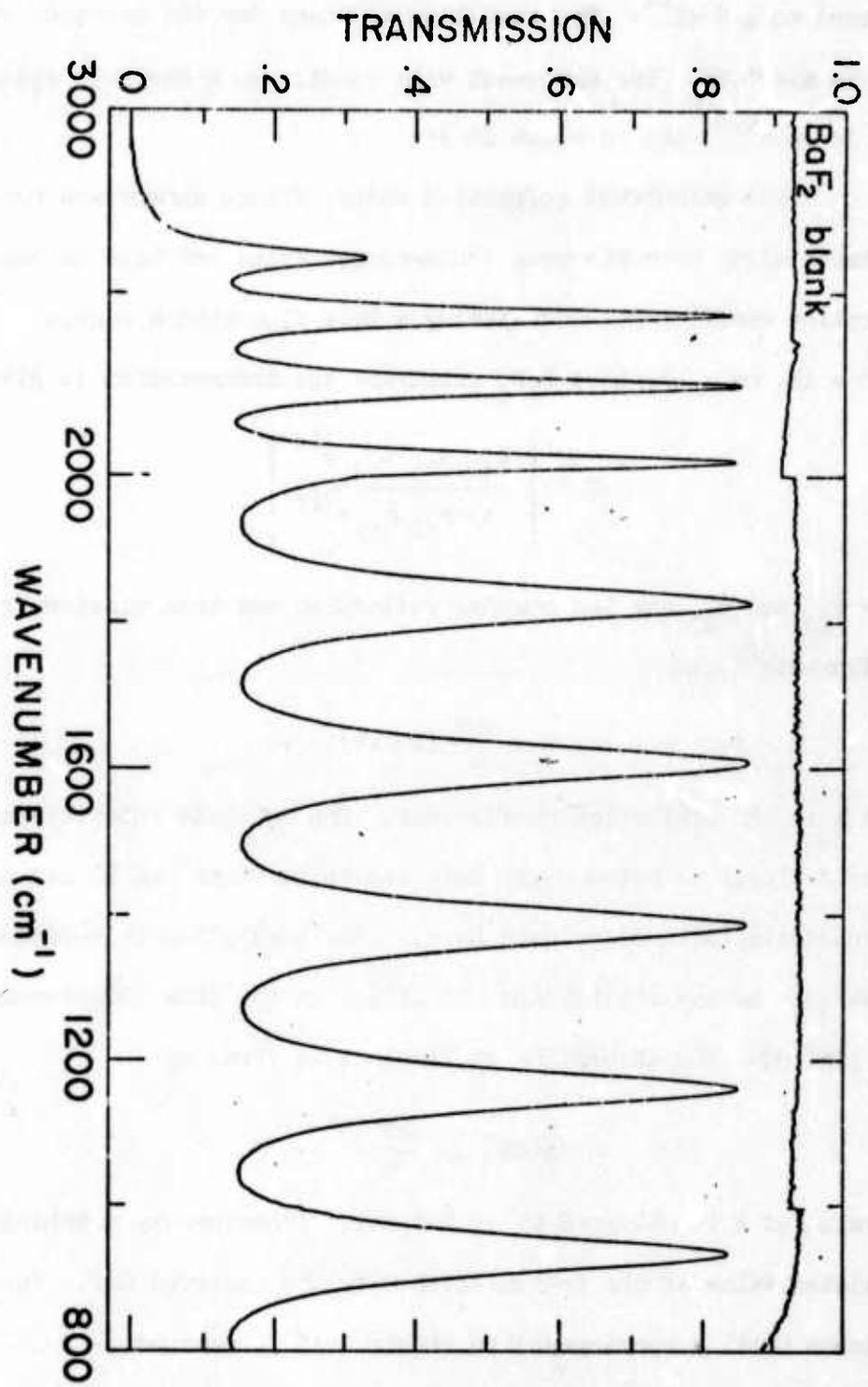

Fig. 1. Transmission data for a 3.7 μm thick PbTe film. A trace from a blank BaF_2 substrate is included. The steps at at 1000 cm^{-1} and 2000 cm^{-1} are due to grating changes.

in the value of d. The fringe index number can be determined unequivocally using an approximate value of the index. The position of the peak can be measured to ± 5 cm^{-1}. The resulting accuracy for the index of refraction is about 2%. The agreement with results on other PbTe epitaxial film work is good[9,21] and is shown in Fig. 2.

The calculated refractive index, fringe number and measured film thickness along with the peak transmission value are used to calculate the absorption coefficient. Consiering a PbTe film with a complex index, $\tilde{n} = n + ik$, on a lossless BaF_2 substrate the transmission is given by

$$T = \left| \frac{t_{12}\, t_{23}\, t_{31}\, e^{i\varphi}}{1 + r_{12}\, r_{23}\, e^{2i\varphi}} \right|^2 \qquad (2)$$

where r_{ij} and t_{ij} are the complex reflection and transmission Fresnel coefficients[22] and

$$\varphi = \frac{4\pi d}{\lambda}(n + ik) \quad , \qquad (3)$$

where k is the extinction coefficient. The multiple interference effect due to reflections between the BaF_2 substrate faces can be neglected for the substrate thicknesses used here. This assumption is verified by the absence of any significant modulation in the film interference curve (see Fig. 1). The absorption coefficient is given by

$$\alpha(cm^{-1}) = \frac{4\pi}{\lambda} k \quad . \qquad (4)$$

The value of k is obtained by an iterative procedure by matching a calculated value of the transmission with the observed one. The iteration continues until a convergence to within 0.1% is reached.

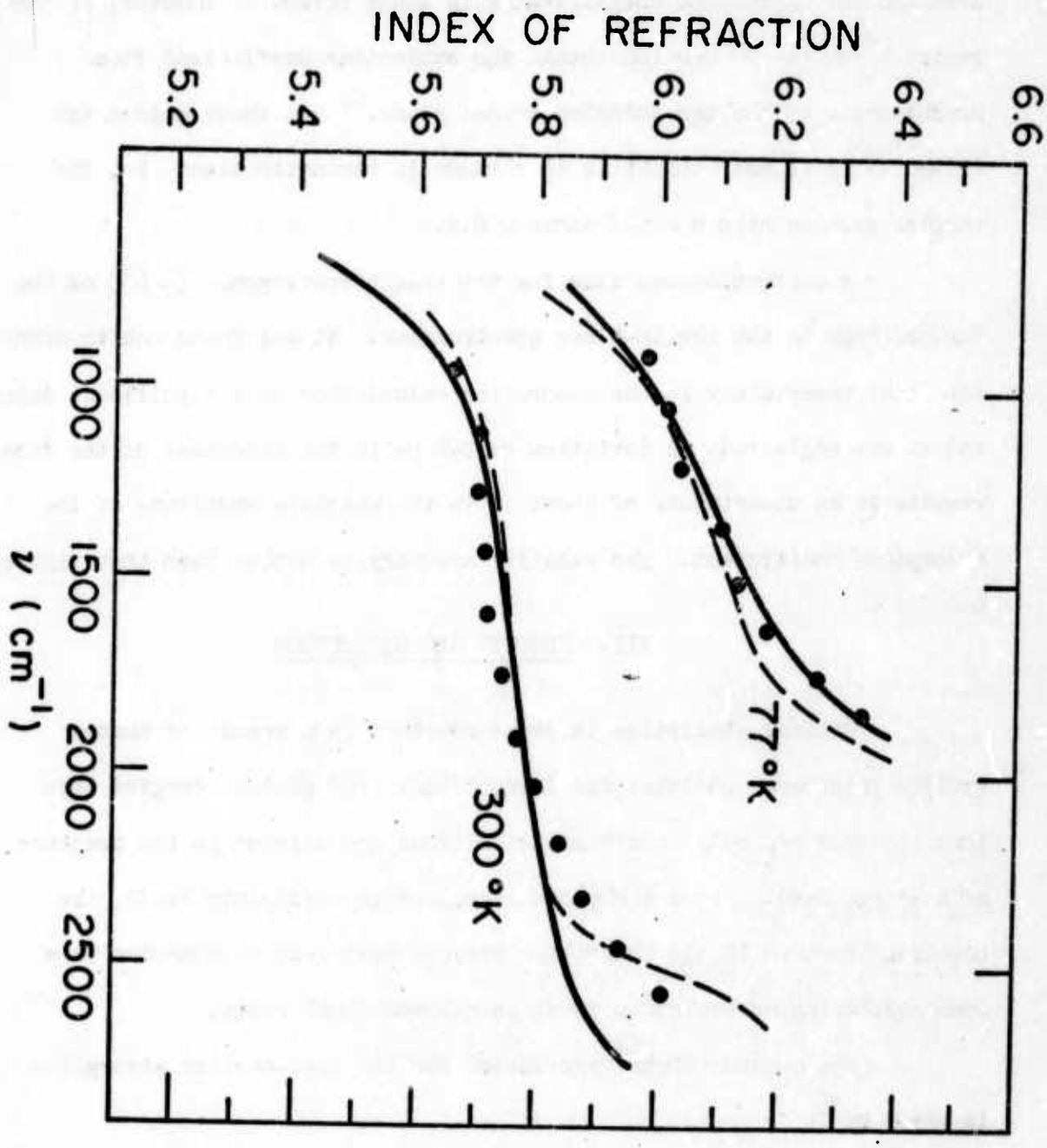

Fig. 2. Index of refraction versus $1/\lambda$ of a film sample. Previous work by Zemel et al.[21] (solid line) and Piccioli[9] (dashed line) for PbTe epitaxial films on NaCℓ is included for comparison.

Generally, it is necessary to measure the intensities of the transmitted and reflected light in order to obtain the index of refraction and the extinction coefficient k in lossy films.[23] However, in the regime $k^2 \ll (n-1)^2$ one can obtain the extinction coefficient from measurements of the transmission maxima alone.[24] At these points the transmission is most sensitive to changes in the extinction. For the samples studied here $n \sim 5\text{-}6$ and $k < 0.1$.

A correction was made for the slight convergence ($\sim 6^\circ$) of the focused beam in the Perkin-Elmer spectrometer. It was found not to affect the total uncertainty in the absorption calculation to a significant extent and so was neglected. A deviation of 0.2 μm in the thickness of the film results in an uncertainty of about 5% in the absolute magnitude of the absorption coefficient. The relative accuracy is better than that figure.

III. RESULTS AND DISCUSSION

Optical absorption in semiconductors is a result of photon excited interband and intraband transitions. For photon energies less than the band gap only intraband transitions are allowed in the presence of a single band. Since the photon momentum is negligibly small, the electron involved in the absorption process must acquire momentum from some scattering mechanism to reach an allowed final state.

The quantum theory expression for the free-carrier absorption is given by[16]

$$\alpha = \frac{e^2}{3 n c \hbar \omega^3 \epsilon_o} \iint W_{k k'}(\omega) \left|\vec{v} - \vec{v}'\right|^2 \left(f_k - f_{k'}\right) \times \delta\left(E_k - E_{k'} + \hbar\omega\right) \frac{d\vec{k}\, d\vec{k}'}{(2\pi)^6} \tag{5}$$

where n is the refractive index, ϵ_o is the permittivity of free space, $W_{k\,k'}(\omega)$ is the scattering matrix element involving photon absorption, f_k is the Fermi function, $\vec{v}$, E_k and $\vec{v}'$, $E_{k'}$ are the initial and final velocities and energy states, respectively.

In the limit that $\hbar\omega \ll E_k$ then

$$f_k - f_{k'} \simeq \frac{\partial f}{\partial E}\hbar\omega \qquad (6)$$

and

$$W_{k\,k'}(\omega) \simeq W_{k\,k'}(0) \quad ,$$

the dc scattering matrix element. Introducing a scattering time involving $W_{k\,k'}(0)$ through the Boltzmann transport equation and assuming $\omega\tau \gg 1$ yields the classical result:

$$\alpha \simeq \alpha_{\text{classical}} = \frac{e^3 N}{4\pi^2 c^3 \epsilon_o n \mu}\left(\frac{\lambda}{m^*}\right)^2 \quad , \qquad (7)$$

where $\mu = e\tau/m^*$ is the dc mobility, m^* is the conductivity effective mass, and N is the free-carrier concentration.

For metals where the electron energies are several electron volts the infrared absorption is described very well by the Drude expression, Eq. (7). However, for the Pb-salt materials the electron energies are less than the infrared photon energy. Table I gives a listing of the characteristic energies for PbTe. The photon energy is much larger than the electron energies: of order kT at room temperature and the Fermi energy E_F at low temperatures.

Quantum theory calculations with electron scattering off acoustic phonons,[17] longitudinal optical phonons,[19] and ionized impurities[18] give free-carrier absorptions going as $\lambda^{1.5-2}$, $\lambda^{2.5}$ and λ^3, respectively.

TABLE I

CHARACTERISTIC ENERGIES IN PbTe (in cm^{-1})

p or n (cm^{-3})	10^{17}			10^{18}		
T(^{o}K)	300	77	10	300	77	10
kT	208	53	7	208	53	7
E_F	non-degenerate	non-degenerate	47	non-degenerate	169	217
$\hbar\omega$(10 μm)	1000	1000	1000	1000	1000	1000

Scattering mechanisms in p-PbTe have been examined recently by Harris and Ridley.[24] Their results indicate that at room temperature for low carrier concentrations polar optical phonon and acoustic phonon scattering are about of equal importance. At higher carrier concentrations ($p > 10^{19}$ cm^{-3}) acoustic phonon scattering dominates and ionized impurity scattering from Pb vacancies becomes important. The presence of an optical phonon interaction is also supported by the observation of an optical phonon branch softening seen in neutron diffraction measurements[26] and the occurrence of paraelectric behavior in the static dielectric constant[27] as the temperature is lowered. At low temperatures ionized defect scattering becomes dominant.

Previously reported optical absorption measurements[5,6] below band gap show a λ^2 dependence suggesting acoustic and optical phonon scattering confirming the transport measurements. The room temperature measurements by Strauss[6] on n-type bulk PbTe are in remarkable agreement with the classical expression, Eq. (7), even though the photon energies are large compared with the electron energy. The temperature dependence of the optical absorption reported in bulk specimens,[5] however, deviates substantially from that predicted classically. The low temperature losses in the Pb-salts are observed to be larger by a factor from 2 to 100 (reference 5 and 7, respectively) than the classical expression predicts.

Figure 3 shows results of optical absorption measurements at room temperature on p-type PbTe epitaxial films. Two types of behavior were noted, characterized by samples 14-3 and 14-4. Absorption curves for a bulk sample[5] and an epitaxial film on NaCl are also included.

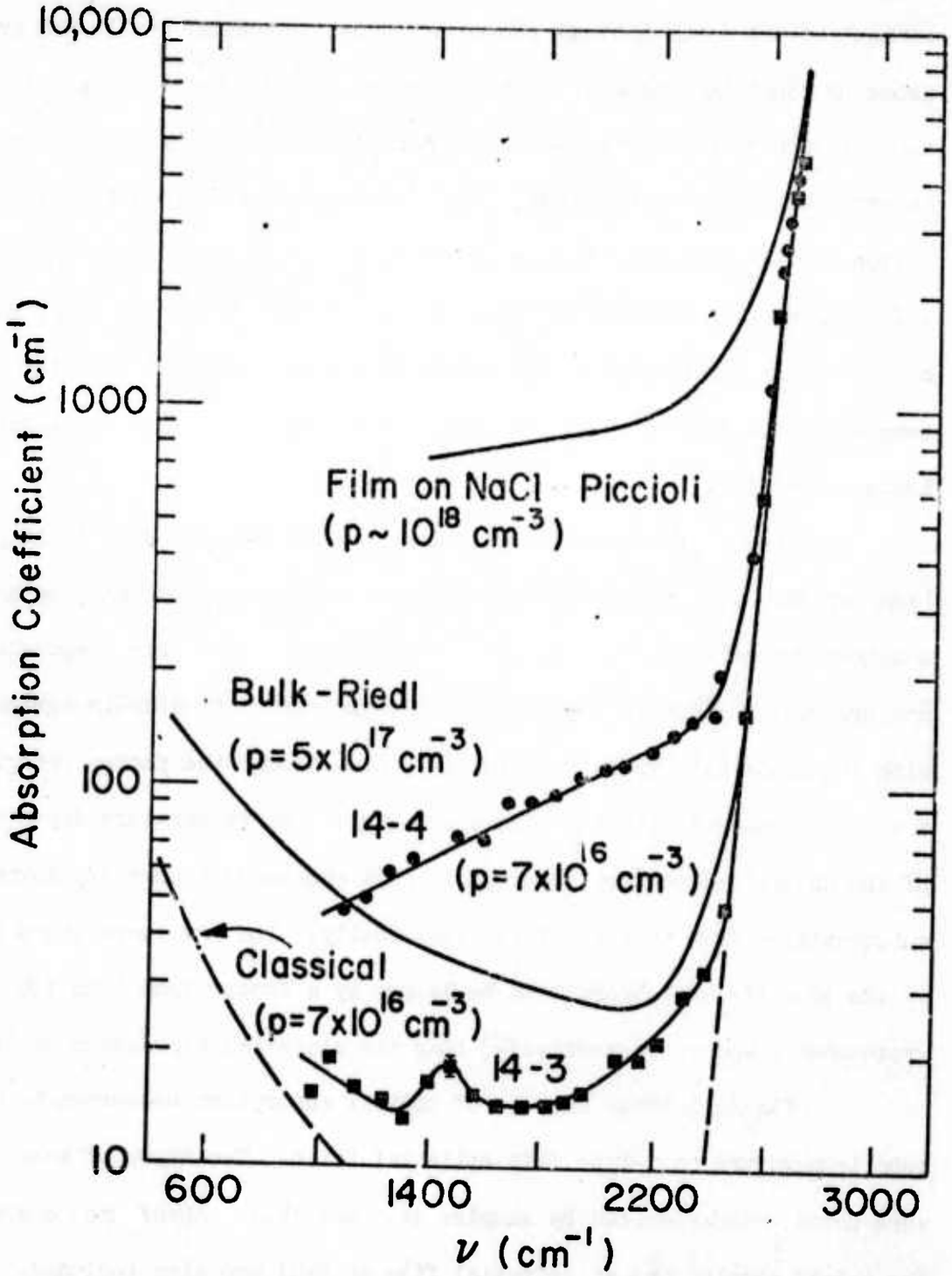

Fig. 3. Absorption spectra of two film samples at room temperature. Previous work on bulk[5] and films on NaCℓ[9] is included. The spectrum of the film on NaCℓ was obtained from reported raw data.

Samples 14-3 and 14-4 were prepared simultaneously. The second number refers only to a location on the substrate holder during film growth. Both samples exhibited nearly identical dc transport properties.

Sample 14-3 shows an absorption at 1000 cm^{-1} (λ = 10 μm) in reasonable agreement with Eq. (7). The energy dependence, however, is not as steep as that observed in bulk samples, even though the transport properties in these films exhibit bulk-like behavior.[3] Sample 14-4 shows a large additional absorption. The exponential decrease in the absorption below the edge suggests the presence of tailing of the band density of states similar to that seen in doped GaAs.[28] A small peak absorption near 1500 cm^{-1} is observed in several "clean" samples, as in 14-3, perhaps associated with a localized level. The energy dependence of the anomalous additonal absorption in 14-4 is similar to that seen by Piccioli[9,29] in films grown on NaCl even though the carrier concentration there was 10^{18} cm^{-3}, which should have given an observable free-carrier contribution.

The full extent of the substrate holder positional dependence on the optical absorption is shown in Fig. 4. A scaled inset of the holder is also included. An order of magnitude variation in the absorption is seen for this group of samples (22-1 to 22-10), from free-carrier like behavior in sample 22-6 to an exponential dependence with opposite slope in 22-7. The transport properties on all samples are similar and do not correlate with absorption data.

Figure 5 gives results of He^4 Rutherford ion-backscattering spectra of the samples 22-6 and 22-7. The only differences occur in the presence of chlorine and perhaps sodium near the surface of the sample 22-7

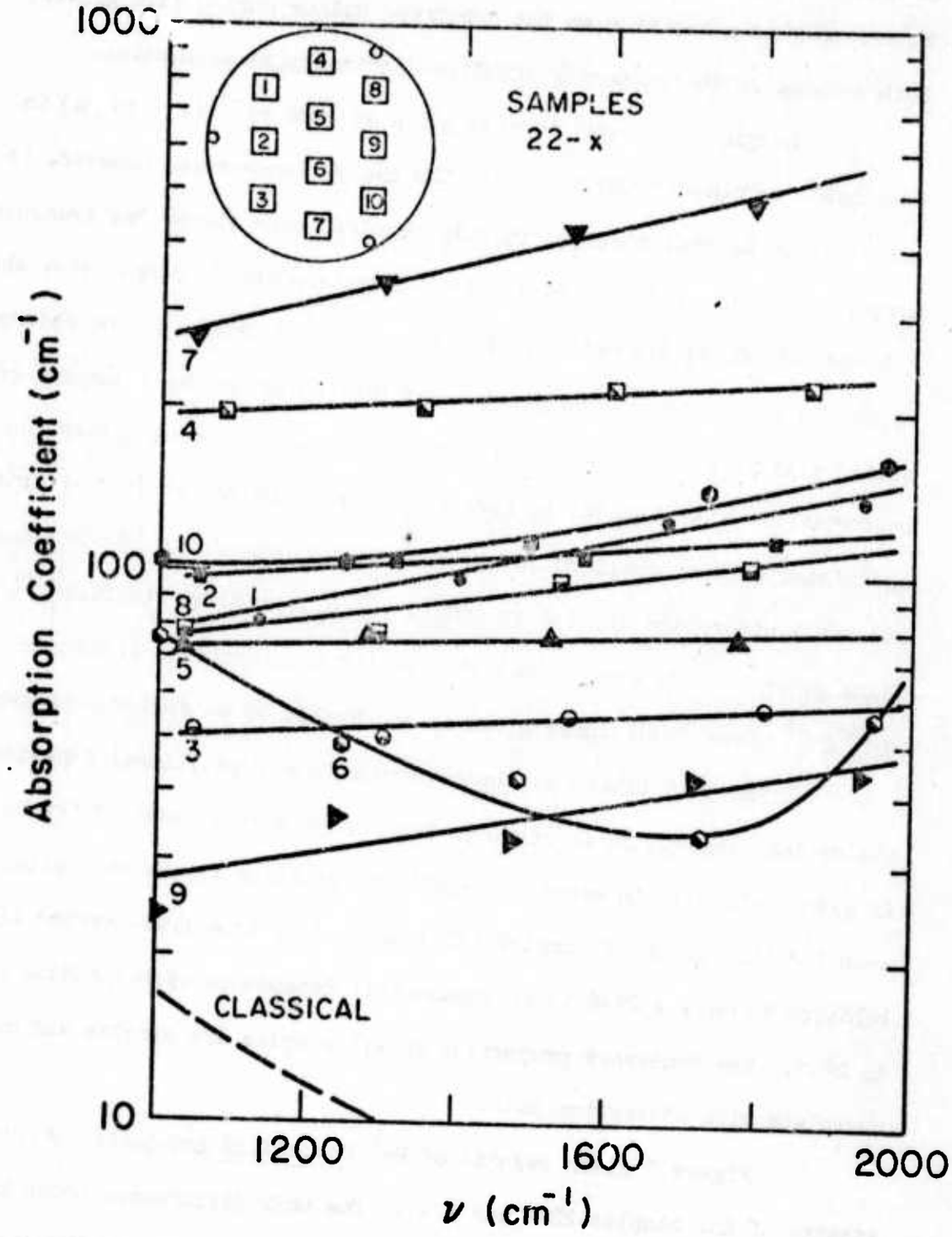

Fig. 4. Absorption spectra of ten samples prepared simultaneouly with numbers referring to sample position during film growth.

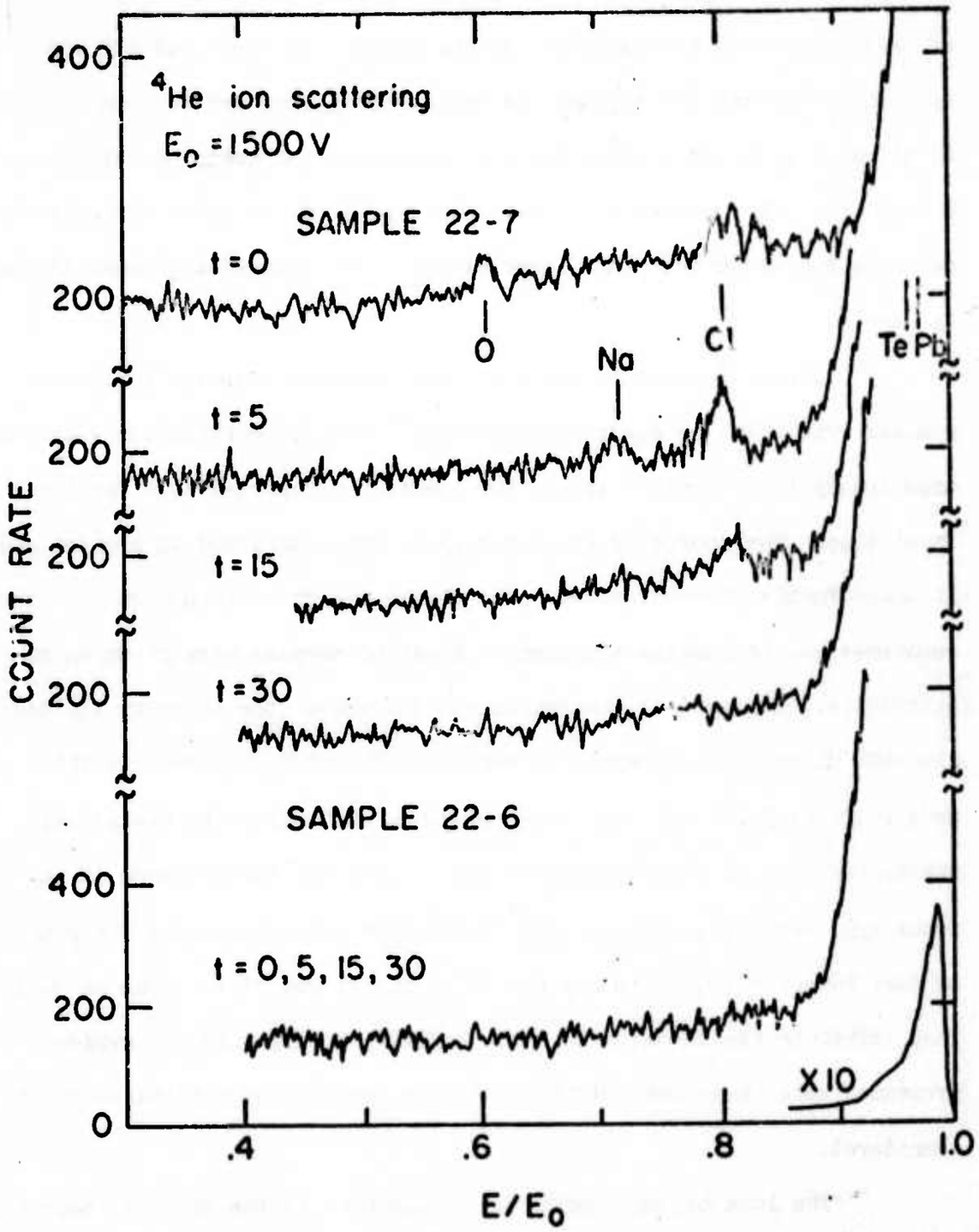

Fig. 5. Ion back-scatter spectra of two samples prepared simultaneously. Sample 22-7 exhibits strong additional optical absorption.

exhibiting strong additional absorption effects. Sample 22-6 appears "clean" (< 1% impurity). The letter t refers to the ion sputtering time in minutes. The spectra from the surface layer indicates the presence of oxygen and chlorine in 22-7. As the surface is sputtered off and consecutive layers are exposed the oxygen disappears and the concentration of chlorine increases. Upon further sputtering the trace of chlorine disappears. The peak at t = 5 min. corresponds to an order of magnitude of a few atomic percent in a layer within a few hundred angstroms of the surface.

Chlorine impurity has also been observed near the surface of similar PbTe films by Auger spectroscopy,[30] but its correlation with the anomalously large optical absorption spectra is reported here for the first time. The source of the impurity is not understood at present and is under further investigation. The strong positional dependence on the substrate holder remains a mystery. A set of samples were grown on KCℓ substrates. The optical absorption spectra showed the impurity limited exponential behavior observed in sample 22-7 on BaF_2 and seen in films on NaCℓ by Piccioli.[9] The high vapor pressure of Cℓ from the heated salt substrates used in the film growth may account for the presence of the impurity. Recently, Duh, et al.[31] have reported evidence for the presence of deep impurity levels in the gap in epitaxial PbS films grown on NaCℓ. They attribute the impurity to SiS. However, in light of the evidence presented here the effect of chlorine from the salt substrates should be considered.

The lack of any temperature dependence in the optical absorption of the PbTe films appears to be associated with the impurity absorption

in all samples. Figure 6 shows the optical absorption in samples 14-3 and 14-4 at 300K and 77K. The behavior predicted by the classical expression, Eq. (7), is included for comparison. The absorption in bulk samples[5] generally decreases by a factor of 4 rather than $\approx$ 10 as predicted by Eq. (7). However, there is no change in the absorption at 77K even for the "clean" sample. This result eliminates an iterpretation of the energy dependence of the room temperature absorption in 14-3 as being caused by indirect transitions from a second valence band.[5,25] One sample was annealed at 350°C in vacuum in the presence of a tellurium pellet. This procedure had the effect of increasing the carrier concentration from 6×10^{16} cm^{-3} to 1.2×10^{18} cm^{-3}. Figure 7 shows the optical absorption coefficient at 300K and 77K. The negative slope of α versus energy for the room temperature measurements suggests a dominant free-carrier contribution. The low temperature measurement demonstrates a reduction of the absorption with a residual impurity absorption remaining. Thus, it is likely that if the impurity content could be eliminated the temperature dependence of the absorption would be similar to that of the bulk PbTe material.

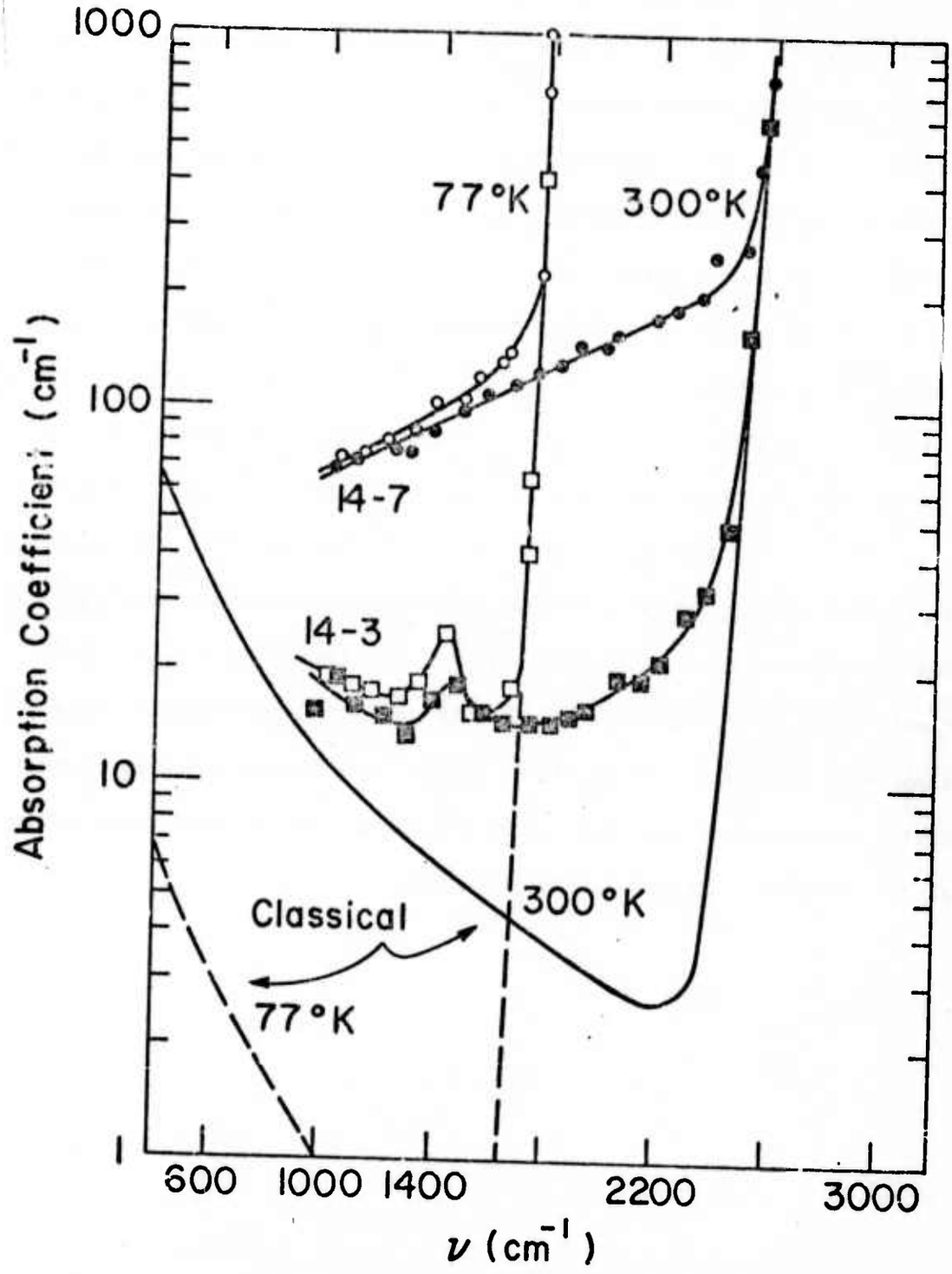

Fig. 6. Absorption spectra of two samples at 300K and 77K. Spectra predicted by the classical Drude theory are included.

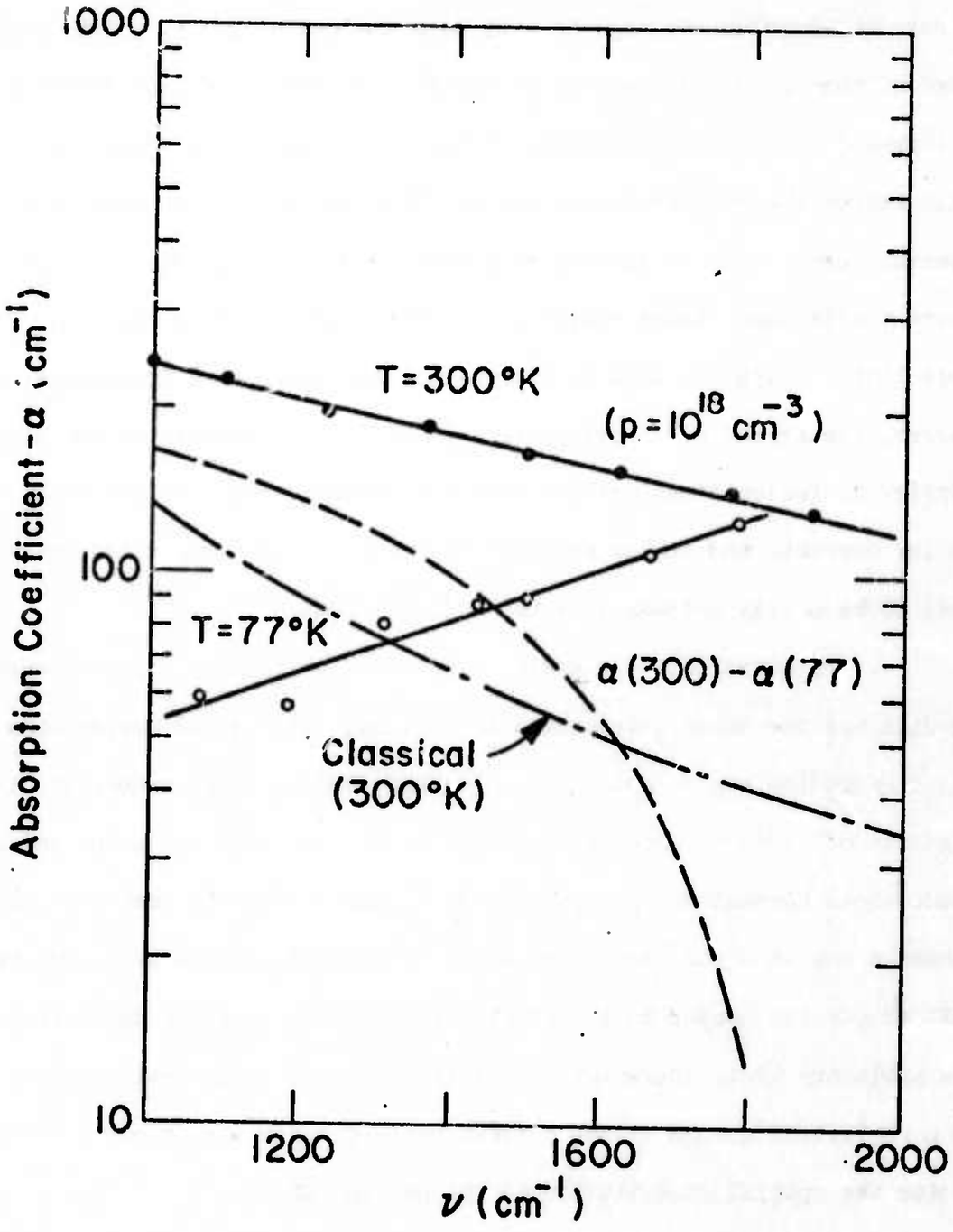

Fig. 7. Absorption spectra of a sample annealed in a tellurium atmosphere measured at 300K and 77K. The difference between the spectra suggests that the temperature dependence arises from the free-carrier contribution.

IV. THRESHOLD GAIN IN ANNEALED SAMPLES

The analysis of threshold conditions in a thin-film laser is complicated by the nonuniform injection. The flow of minority carriers across the junction in Fig. 8a will be a maximum at y = 0, which is the edge of the Pb contact nearest to the Pt electrode, and will decrease as y increases. This result follows since the voltage drop along the film will reduce the voltage across the junction for y > 0. At very high current levels and for films with a high enough resistivity the injection current will come almost entirely from the edge of the Pb contact. In this limit, which was used to analyze the threshold data in unannealed lasers, the spread of minority carriers will be determined by the minority carrier diffusion length rather than the contact area. On the other hand, at low currents and in low resistivity material the current injection will tend to be nearly uniform over the contact area.

To quantitatively estimate the distribution of injected current we will use the model illustrated in Fig. 8b. This model corresponds to dividing up the region under the Pb contact into a large number of discrete elements of width w. Each element has a resistor with $R = \rho w/Ld$ and a diode whose current is $I_n = j_s wL[\exp(eV_n/kT) - 1]$. The number of discrete elements should equal the width of the Pb contact divided by w, but we will choose the number to be infinite in order to simplify the calculation. The arbitrary width increment w must be chosen suitably small so that there is a negligible change in the current between successive diodes. With this choice the spatial distribution is independent of w.

There are two limiting cases of interest: The first occurs when the injection current decreases very rapidly as y increases and is nearly

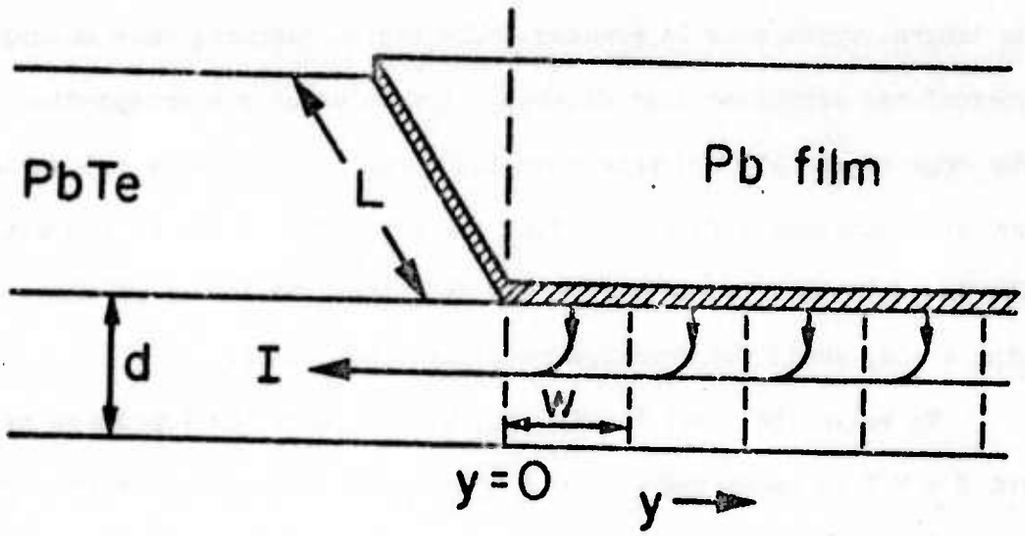

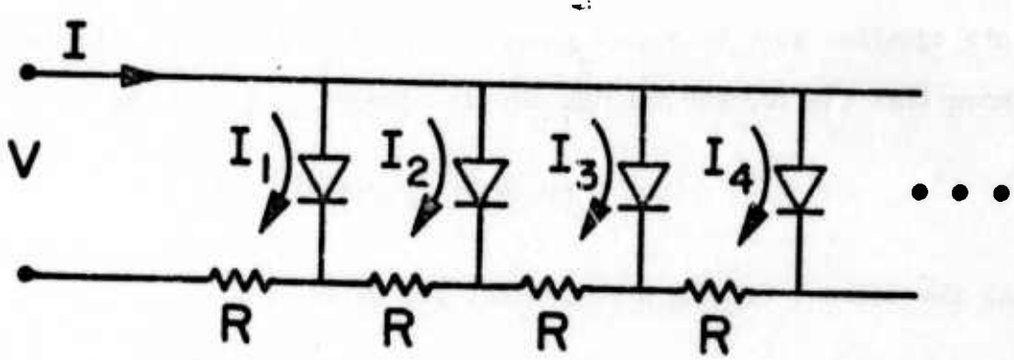

$$R = \frac{\rho w}{Ld}$$

$$I_n = j_s wL \left[\exp(eV_n/kT) - 1\right]$$

Fig. 8. Discrete-element model for calculating the injected current distribution in a thin-film laser.

zero at a value of y corresponding to the far edge of the Pb. In this limit the model of Fig. 8b is valid and the width of the recombination volume is the actual width of the current distribution or the minority carrier diffusion length, which ever is greater. The second limiting case occurs when the current has decreased only slightly at a value of y corresponding to the far edge of the Pb. In this case the model in Fig. 8b is not valid, and the recombination volume is defined by the width of the Pb contact. Our results indicate that unannealed lasers fall into the former of these two limiting cases, while the annealed ones into the latter.

To solve the model in Fig. 8b, we note that the impedance of the network $Z = V/I$ is unchanged when one additional diode-resistor pair is added. Using this result we obtain the following implicit relation for Z as a function of V:

$$VR = Z^2 j_s wL[\exp\{eV(Z-R)/ZkT\} - 1] \quad . \tag{8}$$

This equation must be solved numerically to obtain Z(V). It can then be shown that the current through the n^{th} diode I_n is given by

$$I_n = (IR/Z)\,(1-R/Z)^{n-1} \quad , \tag{9}$$

and the current flowing past a point $y = Nw$ is

$$I(y = Nw) = I - \sum_{1}^{N} I_n = I(1-R/Z)^N \quad . \tag{10}$$

Calculated results for I(y) are shown in Fig. 9 for two current levels and two values of the resistivity. The value $j_s = 8.6 \times 10^{-7}$ A/cm^2, which was estimated from measurements of the zero bias resistance, was used in these calculations. The other parameters are $w = 4$ μm, $d = 4$ μm, $L = 400$ μm.

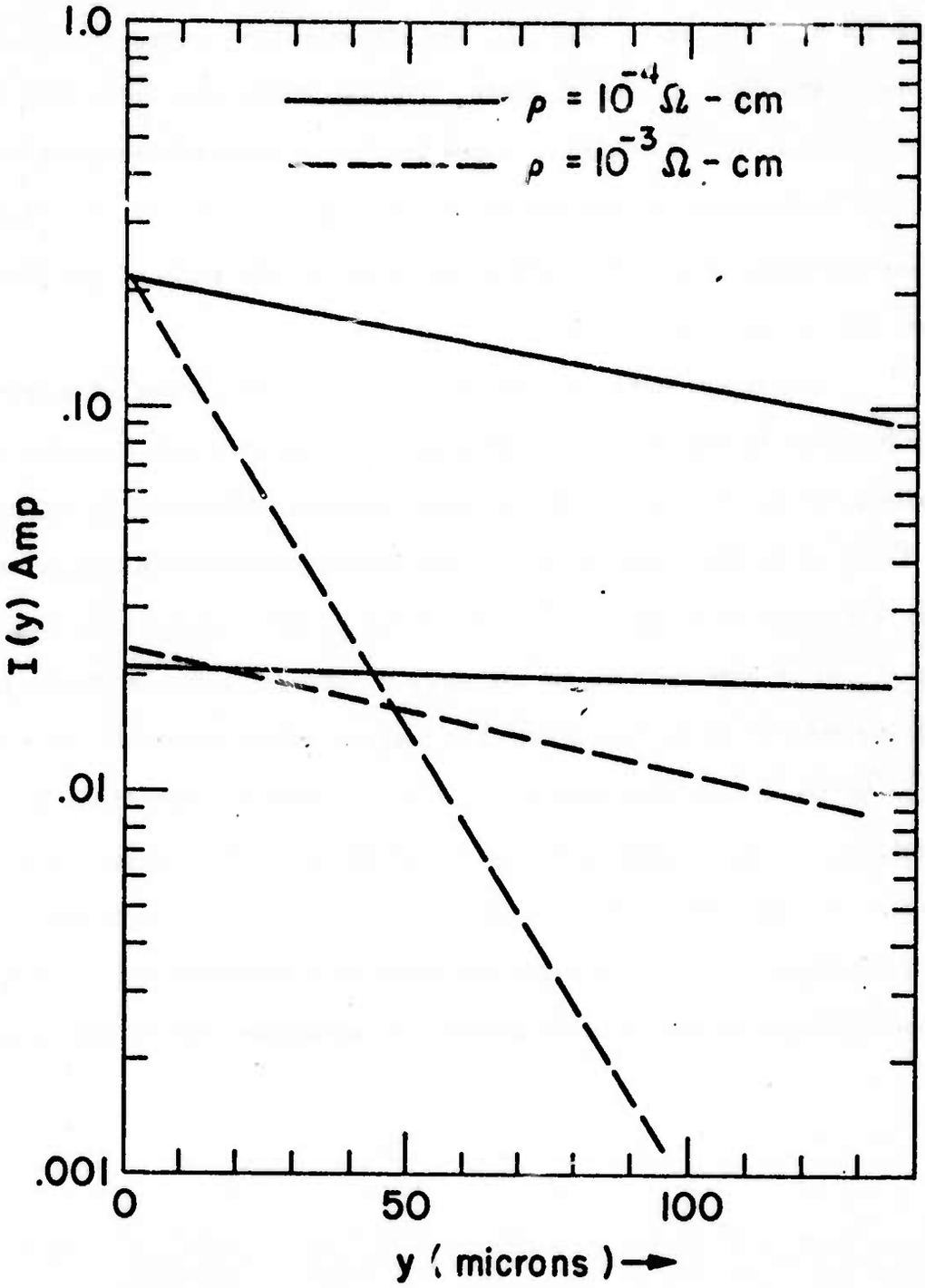

Fig. 9. Current distribution calculated from Eqs. (8) - (10) using the parameters described in text.

The annealed PbTe has a typical 10K resistivity of 10^{-4} Ω-cm, and the laser thresholds for devices made from this material are a few tens of milliamperes. The current distribution at threshold corresponds to the lower solid line in Fig. 9. The recombination volume is, thus, defined by the width of the Pb strip. For the unannealed PbTe, with higher resistivity and higher threshold currents, the current distribution at threshold corresponds to the steeper dashed curve in Fig. 2. The minority carrier diffusion length is a better estimate of the width of the recombination volume for those samples.

We have analyzed the threshold data for five annealed samples using Eq. (25) in Ref. 4. The only parameter that has been changed, besides the recombination volume, is the internal quantum efficiency η, which we have taken to be 5%. This is one of the largest reliable values reported for bulk Pb-salt diode lasers.[13] The result of this analysis is that the optical gain at threshold is in the range 10 - 20 cm^{-1}, i.e. a factor of ten lower than it is in the unannealed samples. This magnitude of gain is similar to the values obtained in a variety of bulk Pb-salt diode lasers. In addition, it is roughly equal to the estimated cavity losses, with no allowance for any appreciable surface scattering. We can therefore conclude that surface scattering is not an important loss mechanism and is probably not the dominant factor in establishing the preference for TE polarization.

V. LOSSES FROM A METAL BOUNDARY

We discuss in this section the attenuation in a metal-clad waveguide resulting from the finite conductivity of the metal. The problem will be treated from a perturbation theory point of view. In the unperturbed problem the metal is assumed to have a pure negative real dielectric constant, and the perturbation corresponds to the addition of a small imaginary component $\delta\epsilon$. It is important to realize that the metal boundary losses cannot be accurately treated as a perturbation on the pure dielectric waveguide. A method using the bouncing-wave, ray-optics picture of the guided modes of a pure dielectric waveguide and incorporating a reduced reflection coefficient r on each bounce to account for the loss from a metal boundary does not account for the large changes in the phase shifts produced by the metal and will not give correct results.

Maxwell's equations can be used to show that the modes of a dielectric slab waveguide follow from the solutions of the following scalar eignevalue equations:

$$\left\{ \frac{\partial^2}{\partial z^2} + \epsilon(z) k_o^2 \right\} E_y(z) = \beta^2 E_y(z) \quad , \qquad \text{TE modes,} \quad (11)$$

$$\left\{ \epsilon(z) \frac{\partial}{\partial z} \frac{1}{\epsilon(z)} \frac{\partial}{\partial z} + \epsilon(z) k_o^2 \right\} H_y(z) = \beta^2 H_y(z) \quad , \text{ TM modes,} \quad (12)$$

where we have assumed no variations in the y direction, x is the direction of propragation, z is the direction normal to the guide surfaces, $k_o = \omega/c$ is the free-space propagation vector at frequency ω, $\epsilon(z)$ is the relative dielectric constant, E_y is the electric field strength for TE modes, H_y is the magnetic field component for TM modes, and all solutions are assumed

to have the dependence $\exp\{i(\beta x - \omega t)\}$. The dielectric constant has the form

$$\epsilon(z) = \begin{cases} \epsilon_1 = -1358 & z > d \\ \epsilon_2 = 41 & 0 \le z \le d \\ \epsilon_3 = 2.02 & z < 0 \end{cases}, \qquad (13)$$

where the values of ϵ_i correspond to Pb, PbTe, and BaF_2, respectively. The conditions at a boundary for Eq. (11) are that E_y and $\partial E_y/\partial z$ are continuous, while those for Eq. (12) are that H_y and $\epsilon^{-1} H_y/\partial z$ are continuous.

We are interested in calculating the change in a bound mode eigenvalue β^2 resulting from a perturbation $\delta\epsilon(z)$ which is pure imaginary for $z > d$ and zero otherwise. For simplicity we consider only first order perturbations and suppress the mode index on the eigenvalues and eigenfunctions. In this case the attenuation coefficient is proportional to the change in β^2. Using first order perturbation theory we find the following results:[32]

$$\alpha_{TE} = \frac{k_o^2 \int_d^\infty dz \, |E_y|^2 \, \delta\epsilon}{\beta_o \int_{-\infty}^\infty dz \, |E_y|^2}, \qquad (14)$$

$$\alpha_{TM} = \frac{\beta_o^2 \int_d^\infty dz \, |H_y|^2 \, \delta\epsilon/\epsilon_1^2 + \int_d^\infty dz \, |\partial H_y/\partial z|^2 \, \delta\epsilon/\epsilon_1^2}{\beta_o \int_{-\infty}^\infty dz \, |H_y|^2/\epsilon_1}. \qquad (15)$$

Calculated results are shown in Fig. 10 for the low order modes. The Pb optical constant is obtained from recent measurements at liquid He temperatures on evaporated Pb films.[33] The use of an infinitely thick

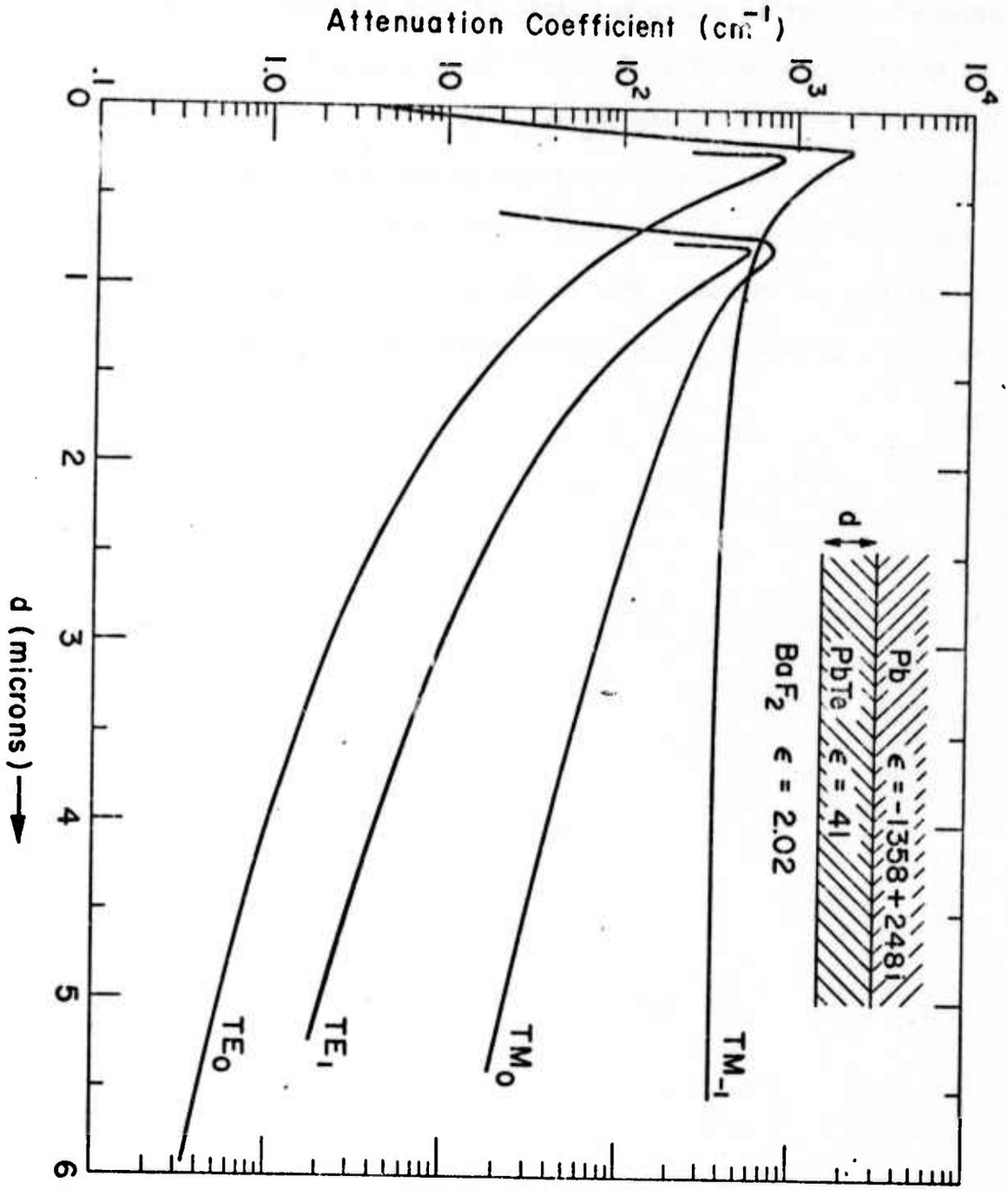

Fig. 10. Loss coefficient in a Pb covered PbTe waveguide for the low order modes. These curves are calculated from Eqs. (14) and (15) using $\delta\epsilon = 248i$.

Pb film is justified for films thicker than a few hundred Å. The TM_{-1} mode is a surface plasmon mode which is characterized by having a constant attenuation coefficient in the limit of very thin and very thick guides and the absence of a cutoff as $d \to 0$.[34] For a 4 μm guide the TE_o attenuation factor is 1 cm^{-1}, while the TM_o value is 40 cm^{-1}. This substantially higher loss for the TM modes is probably the reason these laser show such a strong preference for TE polarization. Surface scattering losses are also higher for TM modes, but the difference is not nearly so great. For the same 4 μm film α_{TM} from surface scattering is roughly 50% larger than α_{TE}.

VI. CONCLUSIONS

Although the optical losses in PbTe films grown on BaF_2 are significantly below those in the films grown on alkali halides, they are still roughly a factor of ten too large for most waveguiding applications. At present the absorption loss in the films grown here are impurity limited, and if the source of the impurity can be verified and removed the optical absorption should be substantially reduced. It is not clear, however, that an absorption as low as 1 cm^{-1} can be achieved in the films, since losses of this magnitude have yet to be demonstrated in bulk material. An attractive alternative approach would be to use some other materials to provide the passive waveguides. A hybrid system employing, for example, Ge or Te waveguides coupling the active Pb-salt devices appears feasible and maintains all the advantages of a thin-film technology with planar processing techniques. Such a system will have advantages in terms of cost, ease of fabrication, and reliability over competing systems using separate bulk crystal lasers and detectors. Films of Ge and Te suitable for waveguiding have been demonstrated,[35,36] but it is not known if these are compatible with the Pb-salt on BaF_2 system.

One goal of this research project has been to determine the feasibility of an integrated optics (IO) heterodyne receiver based on the Pb-salt-on-BaF_2 technology. It appears that such a receiver could be made for operation at 6.4 μm using PbTe for the active devices and another material such as Ge or Te for the passive waveguides. Before definite conclusions regarding the feasibility of a 10 μm IO receiver can be made, however, additional development of thin film active devices using the alloy materials $Pb_{1-x}Sn_xTe$ or $Pb_{1-x}Sn_xSe$ is needed.

A useful heterodyne receiver must be able to operate in the quantum noise limit in which the LO shot noise dominates all other noise sources. Meeting this requirement depends upon all of the system parameters, e.g., detector characteristics, LO power, and bandwidth limitations. In general there will be a trade-off between detector performance and LO power--if the detector is improved, less power is needed in the local oscillator.

For the purpose of evaluating feasibility, the quantum noise limit requirement can be cast in terms of the required LO power for a system using a Pb-salt photovoltaic mixer diode. To determine the detector characteristics we will use results obtained in large area thin-film $Pb_{1-x}Sn_xTe$ devices,[37] scaled down to a 10 μm × 10 μm × 1 μm size. The LO power required is given by[38]

$$P_{LO} \geq \frac{2k(T_M + T'_{IF})\, h\nu}{e^2 \eta} G_D [1 + (f/f_c)^2] \quad , \qquad (16)$$

where k is Boltzmann's constant, T_M is the mixer temperature, T'_{IF} is the effective noise temperature of the IF amplifier, $h\nu$ is the photon energy, e is the electronic charge, η the detector quantum efficiency, G_D is the diode shunt capacitance, f is the IF frequency or bandwidth, $f_c \approx G_D^{\frac{1}{2}}/2\pi C_D R_s^{\frac{1}{2}}$ is the diode cutoff frequency, C_D is the capacitance, and R_s the series resistance. Using $G_D = 5 \times 10^{-7}\ \Omega^{-1}$, $R_s = 10\ \Omega$, $C_D = 1$ pF, $\eta = .2$, $f = 10$ GHz, and $T_M + T'_{IF} = 300$K, condition (16) becomes

$$P_{LO} \geq 5 \times 10^{-5}\ \text{W} \quad .$$

It is expected that powers of this magnitude can be achieved in the 10 μm thin-film materials, since external powers of 10^{-5} W in

thin-film PbTe lasers and 10^{-3} W in bulk $Pb_{1-x}Sn_xTe$ lasers have already been obtained. It is important to realize that the above choice of parameters gives $(f/f_c) \gg 1$. Therefore, a reduction in the required bandwidth from 10 GHz to 1 GHz would reduce the LO power requirement by a factor of 100.

The conclusion is that a 10 μm IO heterodyne receiver using the Pb-salt-on-BaF_2 technology is a very promising system with numerous potential advantages over systems which attempt to couple various discrete bulk-crystal devices. To realize these advantages, however, additional research must be done on the development of a low-loss compatible waveguide material and on the improvement of the active thin-film devices made with the 10 μm Pb-salt alloys.

ACKNOWLEDGMENTS

The authors would like to thank Drs. D. K. Hohnke, H. Holloway and E. M. Logothetis for interesting and informative discussions. We are indebted to Mr. J. L. Parsons for technical advice concerning the operation of the infrared spectrophotometer and Ms. M. Wheeler for measuring the He^4 ion-back scatter spectra. We would also like to thank Mr. K. F. Yeung for assistance in constructing the low-temperature dewars.

REFERENCES

1. H. Holloway, W. H. Weber, E. M. Logothetis, A. J. Varga and K. F. Yeung, Appl. Phys. Letters 21, 5 (1972).
2. E. M. Logothetis, H. Holloway, A. J. Varga and E. Wilkes, Appl. Phys. Letters 19, 318 (1971).
3. H. Holloway, J. Nonmetals (to be published); other references to the materials growth can be found in this paper.
4. W. H. Weber and K. F. Yeung, J. Appl. Phys. 44, 4991 (1973); this paper summarizes the work done during the first reporting period and is included as an Appendix.
5. H. R. Riedl, Phys. Rev. 127, 162 (1962).
6. A. J. Strauss, J. Nonmetals 1, 133 (1973).
7. A. Wycielski, A. Aziza, M. Balkanski, M. Y. Moulin and J. Mycielski, Phys. Stat. Sol. (B) 52, 187 (1972).
8. D. D. Buss and M. A. Kinch, J. Nonmetals 1, 111 (1973).
9. N. Piccioli, Thesis, University of Paris, France, 1971 (unpublished); N. Piccioli, J. M. Besson and M. Balkanski, J. Physique (France) 33, 119 (1972).
10. S. A. Semiletov, I. P. Voronina and E. I. Kortukova, Soviet Physics Crystall. 10, 429 (1966).
11. T. S. Moss, Optical Properties of Semiconductors (Academic Press, Inc., New York 1959) p. 30.
12. T. C. Harman, in Physics of Semimetals and Narrow-Gap Semiconductors, edited by D. L. Carter and R. T. Bate (Pergamon, Oxford, England, 1971) p. 23.

REFERENCES (Cont'd.)

13. R. W. Ralston, I. Melngailis, A. R. Calawa and W. T. Lindley, IEEE J. Quantum Electron. QE-9, 350 (1973).

14. P. Zoutendyk, Ph.D. Thesis, California Institute of Technology, 1968 (unpublished).

15. G. A. Antcliffe and S. G. Parker, J. Appl. Phys. 44, 445 (1973).

16. W. P. Dumke, Phys. Rev. 124, 1813 (1961).

17. R. Rosenberg and M. Lax, Phys. Rev. 112, 843 (1958).

18. S. Visvanathan, Phys. Rev. 120, 376, 379 (1960).

19. V. L. Gurevich, J. G. Lang and Yu. A. Firsov, Soviet Physics-Solid State 4, 918 (1962).

20. S. L. McCarthy, W. H. Weber, M. Mikkor and K. F. Yeung, Scientific Research Staff, Ford Motor Company Technical Report SR-73-129,

21. J. N. Zemel, J. D. Jensen and R. B. Schoolar, Phys. Rev. 140, A330 (1965).

22. M. Born and E. Wolf, Principles of Optics (4th Edition, Pergamon Press, 1970) p. 61.

23. F. Abeles, Prog. in Optics 2, 251 (1963).

24. J. F. Hall, Jr. and W. F. C. Ferguson, J. Opt. Soc. Am. 45, 714 (1955).

25. J. J. Harris and B. K. Ridley, J. Phys. Chem. Solids 33, 1455 (1972).

26. W. Cochran, R. A. Cowley, G. Dolling and M. M. Elcombe, Proc. Roy. Soc. A293, 433 (1966).

27. R. T. Bate, D. L. Carter and J. S. Wrobel, Phys. Rev. Letters 25, 159 (1970).

28. J. I. Pankove, Phys. Rev. 140, A2059 (1965).

REFERENCES (Cont'd.)

29. The experimental raw data reported in Ref. 10 on PbS is in agreement with behavior reported in Ref. 9. Reference 10 reports that PbTe films behave very similarly to PbS films on NaCℓ.

30. H. Holloway (Private Communication).

31. K. Duh, A. Lopez and J. N. Zemel, Bull. Am. Phys. Soc. 18, 325 (1973).

32. W. H. Weber, S. L. McCarthy and G. W. Ford, Appl. Optics, April 1974 (to be published). This reference is included in the Appendix.

33. A. I. Golovashkin, Sov. Phys. JETP 21, 548 (1965).

34. A. Reisinger, Appl. Opt. 12, 1015 (1973).

35. W. S. C. Chang and K. W. Loh, Appl. Opt. 10, 2361 (1971).

36. D. B. Anderson, R. R. August, R. Shubert, J. T. Boyd, Second Quarterly Report, Contract No. N00014-73-C-0297, ARPA Order No. 2327, September 1973.

37. H. Holloway, A. J. Varga, D. K. Hohnke, S. W. Kaiser and P. V. S. Rao, Scientific Research Staff, Ford Motor Company Technical Report SR-73-135.

38. B. J. Peyton, A. J. DiNardo, G. M. Kanischak, F. R. Arams, R. A. Lange and E. W. Sard, IEEE JQE, Vol. QE-8, No. 2, 252 (1972).

PERTURBATION THEORY APPLIED TO GAIN OR LOSS IN AN OPTICAL WAVEGUIDE

W. H. Weber, S. L. McCarthy
Scientific Research Staff, Ford Motor Company, Dearborn, Michigan 48121

and

G. W. Ford
Physics Department, University of Michigan, Ann Arbor, Michigan 48104

We discuss in this letter the use of perturbation theory for calculating the gain or loss in an optical waveguide resulting from a small imaginary component $\delta\epsilon$ introduced into the dielectric constant in or around the guide. In particular we point out the difference in the treatment of TE and TM modes which results from the requirement of self-adjointness of the differential operators to which the perturbation theory is applied.

Maxwell's equations can be used to show that the modes of a dielectric slab waveguide follow from the solutions of the following scalar eigenvalue equations:[1]

$$\left\{\frac{\partial^2}{\partial z^2} + \epsilon(z) k_o^2\right\} E_y(z) = \beta^2 E_y(z) \quad , \qquad \text{TE modes,} \quad (1)$$

$$\left\{\epsilon(z) \frac{\partial}{\partial z} \frac{1}{\epsilon(z)} \frac{\partial}{\partial z} + \epsilon(z) k_o^2\right\} H_y(z) = \beta^2 H_y(z) \quad , \quad \text{TM modes,} \quad (2)$$

where we have assumed no variations in the y direction, x is the direction of propagation, z is the direction normal to the guide surfaces, $k_o = \omega/c$ is the free-space propagation vector at frequency ω, $\epsilon(z)$ is the relative dielectric constant, E_y is the electric field component for TE modes, H_y is the magnetic field component for TM modes, and all solutions are assumed to have the dependence $\exp\{i(\beta x - \omega t)\}$. The conditions at an interface for Eq. (1) are that E_y and $\partial E_y/\partial z$ are continuous, while those

for Eq. (2) are that H_y and $\epsilon^{-1}\partial H_y/\partial z$ are continuous. The waveguide is composed of a layer whose dielectric constant is higher than either of the two media around it. For this case these equations have a finite number of discrete eigenvalues corresponding to solutions which vanish at $z = \pm \infty$, i.e., bound modes, and a continuum of eigenvalues corresponding to radiating modes.

A change $\delta\epsilon(z)$ of the dielectric constant results in a shift of the discrete eigenvalues:

$$\beta^2 = \beta_o^2 + \delta(\beta^2) \quad . \tag{3}$$

For a particular bound mode, in which the unperturbed propagation constant β_o is real, the gain or loss coefficient α produced by $\delta\epsilon$ is

$$\alpha = 2\,\mathrm{Im}\{\beta\} \cong \beta_o^{-1}\,\mathrm{Im}\{\delta(\beta^2)\} \quad , \tag{4}$$

to first order. For simplicity, we consider only first order perturbations and suppress the mode index on the eigenvalues and eigenfunctions.

It has been pointed out that Eq. (1) is identical in form to the one-dimensional Schrödinger equation in which $E_y(z)$ corresponds to the wave function, β^2 to the energy eigenvalue, and $\epsilon(z)k_o^2$ to the potential energy function.[2,3] This correspondence allows one to use the well known result from bound state perturbation theory that the first order change in the eigenvalue $\delta(\beta^2)$ caused by a small change $\delta\epsilon(z)$ in the dielectric constant is given by the expectation value of the perturbation in the unperturbed state:[3,4]

$$\delta(\beta^2)_{TE} = k_o^2 \langle E_y, \delta\epsilon\, E_y\rangle_{TE} / \langle E_y, E_y\rangle_{TE} \quad , \tag{5}$$

where the inner product is defined as

$$\langle f,g\rangle_{TE} = \int_{-\infty}^{\infty} dz\, f^*(z)\, g(z) \quad . \tag{6}$$

Note that the validity of this result depends upon the fact that the differential operator in Eq. (1) is self-adjoint using the inner product defined in Eq. (6).[4]

For the slab dielectric waveguide $\epsilon(z)$ is piecewise constant and $H_y(z)$ for the TM modes also satisfies Eq. (1), except for the different conditions at the interfaces. Because of this simplification one is tempted to expect a result similar to Eqs. (5) and (6) for the change in the TM mode eigenvalues.[5] This is not the case, however, for the following two reasons:

First, the operator for the TM modes is not self-adjoint as it appears in Eq. (2). It can be made self-adjoint by introducing a change of variable as done by McKenna[1] or, which is equivalent, by simply introducing a new inner product:

$$\langle f,g\rangle_{TM} = \int_{-\infty}^{\infty} dz\, \epsilon(z)^{-1} f^*(z)\, g(z) \quad . \tag{7}$$

Second, even though $\epsilon(z)$ is piecewise constant, the derivative term gives a nonzero contribution to $\delta(\beta^2)_{TM}$. That is, the operator on the left hand side of Eq. (2) will, to first order in $\delta\epsilon$, contain the perturbing terms:

$$\delta\epsilon \frac{\partial}{\partial z}\frac{1}{\epsilon}\frac{\partial}{\partial z} - \epsilon \frac{\partial}{\partial z}\frac{\delta\epsilon}{\epsilon^2}\frac{\partial}{\partial z} + \delta\epsilon\, k_o^2 \equiv -\left(\frac{\partial}{\partial z}\frac{\delta\epsilon}{\epsilon}\right)\frac{\partial}{\partial z} + \delta\epsilon\, k_o^2 . \tag{8}$$

Bound state perturbation theory now tells us that the first order change in β^2 for the TM modes is given by the expectation value of the perturbation (8) in the unperturbed state, using the scalar product (7):[4]

$$\delta(\beta^2)_{TM} = \frac{k_o^2 \langle H_y, \delta\epsilon H_y \rangle_{TM} - \langle H_y, \left(\frac{\partial}{\partial z}\frac{\delta\epsilon}{\epsilon}\right)\frac{\partial H_y}{\partial z}\rangle_{TM}}{\langle H_y, H_y\rangle_{TM}} \quad . \qquad (9)$$

This result is similar to Eq. (5) except for an extra term and a different definition for the inner product. For the dielectric slab waveguide the term involving the derivative of $\delta\epsilon/\epsilon$ vanishes except at an interface where it has a delta-function character giving a finite contribution. An alternative expression for $\delta(\beta^2)_{TM}$, which does not involve such delta-function contributions, can be obtained from Eq. (9) by using Eq. (2) and integrating by parts. The result is

$$\delta(\beta^2)_{TM} = \frac{\beta_o^2 \int_{-\infty}^{\infty} dz |H_y|^2 \delta\epsilon(z)/\epsilon(z)^2 + \int_{-\infty}^{\infty} dz |\partial H_y/\partial z|^2 \delta\epsilon(z)/\epsilon(z)^2}{\int_{-\infty}^{\infty} dz |H_y|^2/\epsilon(z)} \quad . \qquad (10)$$

This expression is, of course, equivalent to that given in Eq. (9). We write it in this form to point out that it is identical to the expression given recently by Reisinger[6] for TM modes, which was derived by energy loss considerations. The advantage of using perturbation theory to calculate α, rather than working with the energy loss in Maxwell's equations, is that it is somewhat simpler and has a well developed formalism for calculating higher order corrections and estimating errors.

For modes far away from cutoff $\beta_o^2 |H_y|^2 \gg |\partial H_y/\partial z|^2$, and the second term in the numerator of Eq. (10) can be neglected compared with the first. Near cutoff, however, the two terms will tend to be of comparable magnitude. In general the influence of the second term will be increased when the dielectric discontinuities between the guide and the surrounding media are increased.

REFERENCES

1. J. McKenna, Bell System Tech. J. 46, 1491 (1967).

2. P. K. Tien, Appl. Opt. 10, 2395 (1971).

3. K. O. Hill, A. Watanabe and J. G. Chambers, Appl. Opt. 11, 1952 (1972).

4. See for example Eugen Merzbacher, Quantum Mechanics (John Wiley & Sons, Inc., New York, 1970, 2nd edition), Chapter 17.

5. This is apparently the reasoning used in deriving Eqs. (A3) in Ref. 3.

6. A. Reisinger, Appl. Opt. 12, 1015 (1973).

Waveguide and luminescent properties of thin-film Pb-salt injection lasers*

W. H. Weber and K. F. Yeung

Scientific Research Staff, Ford Motor Company, Dearborn, Michigan 48121
(Received 30 May 1973; in final form 6 July 1973)

We describe the waveguide properties of the asymmetric dielectric slab formed by a very-high-index film on a low-index substrate. The analysis is appropriate for Pb-salt films grown on fluorite structure substrates. The mode reflectivities, surface scattering losses, and gain enhancements for the low-order TE and TM modes are considered. The stronger confinement of the TM modes leads to larger gain enhancements than for the TE modes. For the film thicknesses of interest, 2–4 μm, the TE and TM mode reflectivities are comparable. Using the theory of Tien, the TE modes show substantially lower surface scattering losses than TM modes of the same order. The magnitude of this loss, however, depends on an unknown parameter σ, the variance of the surface height. Experimental results are presented for thin-film diode lasers made with Pb Schottky barriers on p-type PbTe (index 6.4) grown epitaxially on BaF_2 substrates (index 1.42). The spontaneous emission at 77 °K is shown to agree with the band-band recombination model, assuming k conservation. Laser emission at 6.5 μm, both pulsed and cw, is observed at 10–15 °K. Well above threshold the spectra generally show two dominant modes spaced by $\simeq 1.4$ meV. This splitting is attributed to a strain-induced shift of the energy bands. Using the deformation potentials for PbTe the observed splitting leads to an estimate -2×10^{-4} of the strain component in the [111] direction normal to the film surface. All observed laser lines are TE polarized. An analysis is made of the gain and loss parameters at threshold. The optical gain is estimated from the measured current and quantum efficiency, while the free carrier and reflection losses are calculated from the device parameters. The remaining losses can then be estimated from the threshold condition. If these losses are attributed to surface scattering, the analysis can be used to give an upper limit on σ of 0.03–0.06 μm. In every case the surface scattering loss is dominant in establishing the laser threshold, which is consistent with the strong preference shown for TE modes.

I. INTRODUCTION

Laser action in the Pb-salts was first observed in 1964 by Butler *et al.*,[1] who reported diode lasers in PbTe. Subsequently, laser diodes have been made in PbSe [2] and PbS,[3] as well as in most of the pseudobinary alloys such as $Pb_{1-x}Sn_xTe$ and $Pb_{1-x}Sn_xSe$.[4] These lasers have been made from bulk crystalline samples grown by vapor transport or Bridgman techniques, and a review of this work is given in a recent paper by Harman.[5] The bulk devices consist of a rectangular crystal with cleaved (100) end faces forming a Fabry-Perot cavity. Due to the weak confinement of the laser beam in the direction normal to the junction plane (typically 40—50 μm at liquid-helium temperatures), these devices approximate a volume laser with nearly plane-wave propagation assumed between the end reflectors. Previous analyses of the gain and loss characteristics of these lasers have generally used the volume laser approximation.[5–7]

Recent studies of the epitaxial growth of IV-VI compounds on fluorite structure substrates have shown that films of excellent crystalline quality can be achieved.[8] These films have yielded high-quality infrared detectors[9] and field-effect transistors as well as lasers.[10] The primary purpose of this paper is to discuss the light emission and laser characteristics of the thin-film lasers. Since typical film thicknesses are several microns—i.e., on the order of the emission wavelength—the waveguiding properties of the films must be considered in determining the mode preference and threshold conditions for the lasers. The increased electrical and optical confinement afforded by the thin films enhances the optical gain significantly over that obtained in bulk devices. At the same time, however, the cavity losses are increased by the introduction of surface scattering.

In Sec. II we present an analysis of the properties of the asymmetric dielectric waveguide formed by a high-index semiconductor film on a low-index substrate. Surface scattering losses, reflection losses, and gain enhancement for the low-order TE and TM modes are considered. Calculations are presented for PbTe films (index 6.4) on BaF_2 substrates (index 1.42), but the results should apply to other systems with comparably large index differences. The stronger optical confinement associated with the TM modes can lead to reflectivities and gain enhancements larger than those for the corresponding TE modes. On the other hand, the TE modes always show lower surface scattering losses than TM modes of the same order. To treat these surface losses, we will use the simple theory of Tien based on the Rayleigh criterion.[11,12] This theory involves a single unknown parameter σ, the variance of the surface height, which we assume to be the same for both surfaces. For the mode reflectivity calculations we will use an extension of the method employed by Reinhart *et al.* to treat a similar problem in double-heterostructure lasers.[13] For thick films we find results very similar to theirs, with the TE modes showing higher reflectivities than the TM modes. For thinner films, however, there is no clear preference.

We present the experimental results in Sec. III. These include a brief description of the sample preparation, an analysis of the spontaneous emission spectrum at 77 °K, and measurements of the spectra and polarization of the laser emission at liquid-helium temperatures. An important step in the sample preparation, which was not used in previous devices,[10] is the use of

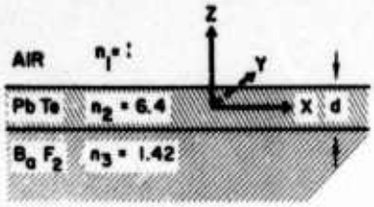

FIG. 1. Geometry for PbTe waveguide on BaF_2 substrate.

a photoresist etching technique to define the ends of the optical cavity. This produces much better edges than those obtainable on the as-grown films using close-spaced evaporation masks. Minority-carrier injection is achieved with Pb Schottky barriers on p-type PbTe films. The spontaneous emission spectrum is fit quite well with the band-to-band recombination model assuming vertical transitions. Under high-current conditions at liquid-helium temperatures, some devices show two distinct laser emission lines with a separation much larger than the cavity mode spacing. This splitting is explained in terms of a strain-induced shift of the energy bands. Using a deformation potential calculation leads to the estimate -2×10^{-4} for the strain component normal to the film surface.

In Sec. IV we give an analysis of the gain and loss parameters at the lasing threshold. The optical gain at threshold is estimated from the diode current using the band-to-band recombination model. The free-carrier absorption is calculated from the measured material parameters, and the reflection losses are determined from the results of Sec. II. By using these results, the surface scattering loss can be estimated if it is assumed that there are no other loss mechanisms. This analysis gives an upper limit for σ in the range 0.03–0.06 μm. In all cases, the estimated gain at threshold is much greater than the sum of the free-carrier and reflection losses. This indicates that the additional losses, which we attribute to surface scattering, are dominant in determining the laser threshold.

II. WAVEGUIDE PROPERTIES

A. Description of the modes

Since the general formalism for treating the waveguide modes of the asymmetric dielectric slab is well known,[11,14] we will omit derivations and give only those results essential for defining the notation and understanding the subsequent discussion. For the two-dimensional geometry shown in Fig. 1, the guided modes follow from the solutions of the homogeneous Maxwell equations which vanish at $z=\pm\infty$. The solutions separate into transverse electric (TE) and transverse magnetic (TM) modes. The appropriate equation for the TE mode is

$$\left(\frac{d^2}{dz^2}+n_i^2\frac{\omega^2}{C^2}\right)E_y=\beta^2E_y, \tag{1}$$

where β is the propagation constant in the x direction, n_i is the refractive index of the ith medium, E_y is the electric field strength (which has only a y component), ω is the angular frequency, and c is the velocity of light. In our problem, with the refractive index stepwise constant in all directions, H_y for TM modes also satisfies Eq. (1).

The solutions result from matching the boundary conditions at the dielectric interfaces and solving the resulting eigenvalue equation. Following Tien,[11] the transverse field components for TE and TM modes can be written in the form

$$A\exp[i(\beta x-\omega t)]\begin{cases}\cos(k_2z_{12})\exp[-k_1(z-z_{12})], & z>z_{12}\\ \cos(k_2z), & z_{12}>z>-z_{23}\\ \cos(k_2z_{23})\exp[k_3(z+z_{23})], & -z_{23}>z\end{cases} \tag{2}$$

where z_{12} and $-z_{23}$ are the values of z at the upper and lower surfaces, respectively, $k_{1,3}=(\beta^2-n_{1,3}^2k^2)^{1/2}$, $k_2=(n_2^2k^2-\beta^2)^{1/2}$, and we have introduced the free-space wave vector $k=\omega/c=2\pi/\lambda$. The allowed values of the propagation constant β are determined from the equation

$$z_{12}+z_{23}=d, \tag{3}$$

where d is the film thickness. For the TE modes, z_{12} and z_{23} are given by

$$\begin{aligned}k_2z_{12}&=\arctan(k_1/k_2),\\ k_2z_{23}&=\arctan(k_3/k_2)+m\pi,\end{aligned} \tag{4}$$

while for the TM modes we have

$$\begin{aligned}k_2z_{12}&=\arctan(n_2^2k_1/n_1^2k_2),\\ k_2z_{23}&=\arctan(n_2^2k_3/n_3^2k_2)+m\pi,\end{aligned} \tag{5}$$

where $m=0,1,2,\ldots$, is the mode index. The roots of Eq. (3) are generally found by numerical techniques. Note that defining the fields by expression (2) requires the position $z=0$ be different for each mode.

We show in Fig. 2 plots of the propagation constant β as a function of the guide thickness d for the first three TE and TM modes. The frequency used in these calculations corresponds to a free-space wavelength of 6.5 μm. Also shown as dashed curves are plots of the equation

$$d=(m+1)\pi/(n_2^2k^2-\beta^2)^{1/2}, \tag{6}$$

which would describe the solutions for a waveguide with perfectly conducting walls, i.e., no penetration of the

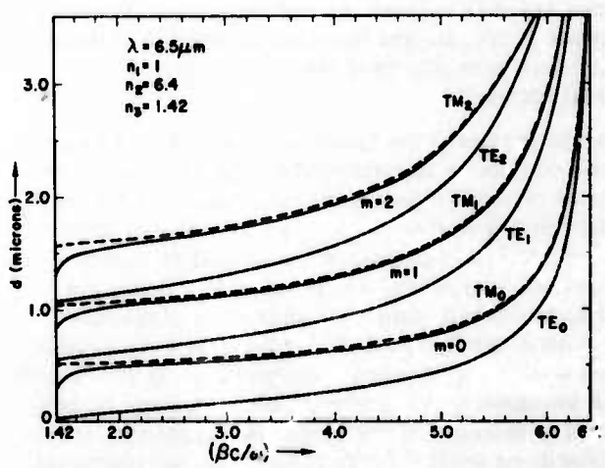

FIG. 2. Film thickness vs $\beta c/\omega$ for the low-order modes. The dashed curves are solutions corresponding to no penetration of the fields into the surrounding media.

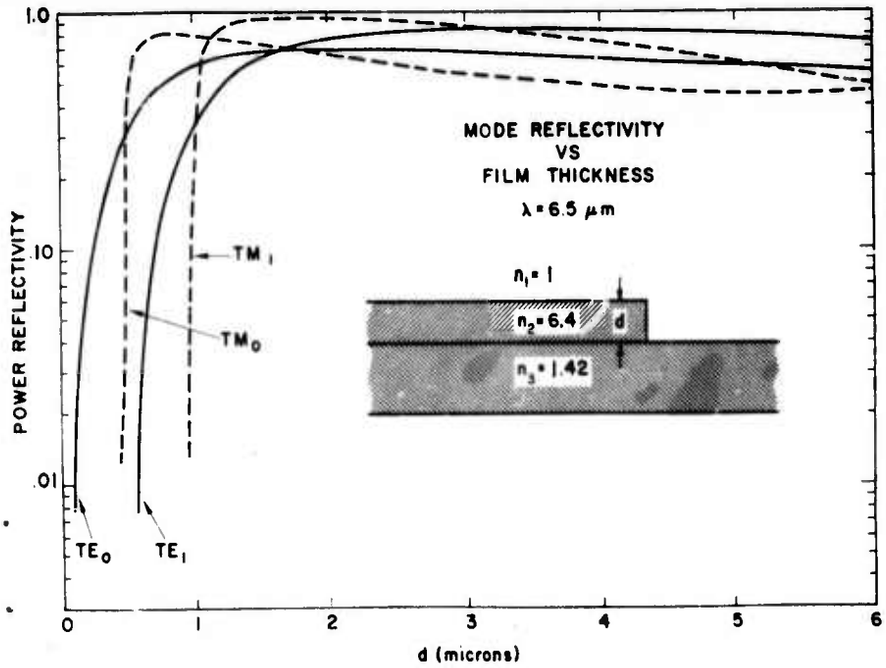

FIG. 3. Power reflectivity vs film thickness for the first two TM and TE modes, calculated from the square of Eq. (9).

fields into the surrounding media. The purpose of these plots is to indicate that for most values of β the TM modes are very closely fit by Eq. (6) and are, thus, much more strongly confined than the TE modes. This feature leads to important differences in the mode reflectivity and gain enhancement as we will demonstrate in the remainder of this section.

B. Mode reflectivity

To determine the exact reflectivity of a waveguide mode requires the solution of a difficult boundary value problem, and no attempt at such a solution will be given here. Instead, we will use a physical optics argument to obtain an estimate of the reflectivity. This method is the same as one used previously to estimate the mode reflectivities in double-heterostructure lasers.[13] Our results will differ from that work in two respects: We will use the exact mode profiles in the calculations, rather than a Hermite-Gaussian approximation, and we will introduce a truncated Fourier transform to take into account the evanescent tails of the modes extending into the surrounding media.

We assume the semiconductor film is terminated with a surface in the zy plane. The incident field illuminating the guide end is written as a Fourier decomposition $S(k_z)$ in the z direction of the transverse field component. For a TE mode, we define $S(k_z)$ by

$$S(k_z) = \int_{-\infty}^{\infty} E_y(z) \exp(-ik_z z)\, dz. \tag{7}$$

Each Fourier component corresponds to a plane or evanescent wave incident on the film-air boundary at the guide end. The evanescent tails on $E_y(z)$, however, will not "see" the end of the guide as effectively as the rest of the mode. To take this effect into account, we introduce a truncated transform

$$S_t(k_z) = \int_{-z_{23}}^{z_{12}} E_y(z) \exp(-ik_z z)\, dz. \tag{8}$$

We can now find the reflected fields by multiplying each of these components by the appropriate Fresnel coefficient $F(k_z)$. This method assigns zero reflectivity to the evanescent tails and will probably underestimate the total reflected wave. We expect it to be a very good approximation for large d, and for small d it is a physically reasonable way of treating the mode reflectivities near cutoff. Finally, the amplitude reflectivity r is given by projecting out the original mode from the reflected waves

$$r = \left(\int_{-\infty}^{\infty} S^*(k_z) S_t(k_z)\, dk_z\right)\left(\int_{-\infty}^{\infty} S^*(k_z) S(k_z)\, dk_z\right)^{-1}. \tag{9}$$

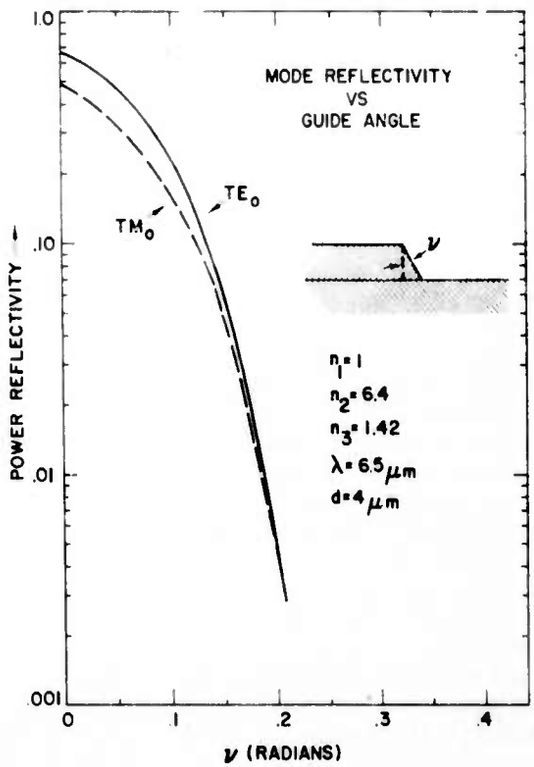

FIG. 4. Power reflectivity for zero-order modes vs the guide angle defined in the figure.

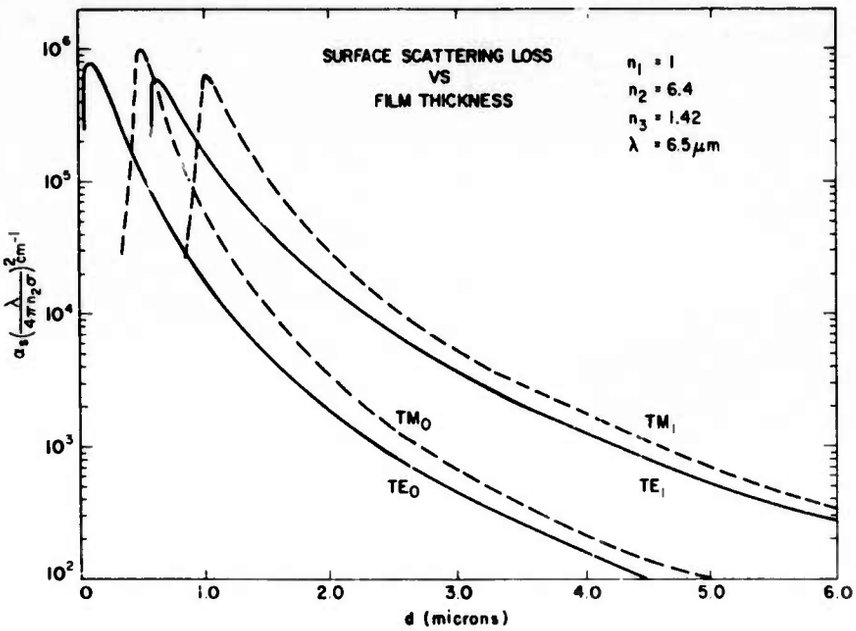

FIG. 5. Surface scattering loss coefficient defined in Eq. (12) vs the film thickness for the first two TE and TM modes.

The Fresnel coefficient for TE modes is given by

$$F_{TE}(k_x) = (\kappa_2 - \kappa_1)/(\kappa_2 + \kappa_1), \tag{10}$$

where $\kappa_i = (n_i^2 k^2 - k_x^2)^{1/2}$. For the TM modes we replace $E_y(z)$ by $H_y(z)$ and use the Fresnel coefficient F_{TM}:

$$F_{TM}(k_x) = (n_1^2\kappa_2 - n_2^2\kappa_1)/(n_1^2\kappa_2 + n_2^2\kappa_1). \tag{11}$$

In Fig. 3 we show computer results for the mode reflectivities of the first two TE and TM modes, calculated by using Eqs. (7)–(11). The integrals in Eqs. (7) and (8) can be evaluated explicitly, but the one in Eq. (9) must be done numerically.

For thick films the simple formulas in Ref. 13 give roughly the same results; e.g., the reflectivity values of the zero-order modes at $d = 6$ μm are within 10% of those in Fig. 3. However, for the data we will be presenting, typical values are $d = 2$–4μm, and for this range of thicknesses the results from the two models are very different.

It is also of interest to consider the reflectivity of a guide with a nonrectangular end. Films grown by evaporation through a mask will tend to have a tapered edge due to the finite source size and the separation between substrate and mask. We assume this fuzzy edge can be approximated by a plane surface whose normal is in the xz plane making a small angle ν with the x axis. It is then a simple matter to modify Eq. (9) for this model. The resulting reflectivity as a function of ν is shown in Fig. 4 for the zero-order modes of a 4-μm film. For thinner films, the reflectivity falls off less rapidly and for thicker films more rapidly than shown in the figure. We have found that an edge defined by an evaporation mask will tend to have a tapered region at least 1 μ wide, and it is clear from Fig. 4 that such an edge will introduce severe reflection losses. To get around this problem we have been using an etching technique to define the laser edges.

C. Surface scattering losses

We will treat the surface scattering losses by using the simple theory based on the Rayleigh criterion for reflection losses from slightly rough surfaces.[11,15] Although this theory is fairly crude in that it ignores the mode properties of the guide, it is based on sound physical arguments and is easy to apply. In addition, it is the only theory that has been successfully applied to experiments on losses in an optical waveguide.[12]

To calculate the loss, we first decompose the transverse field component inside the guide into two plane

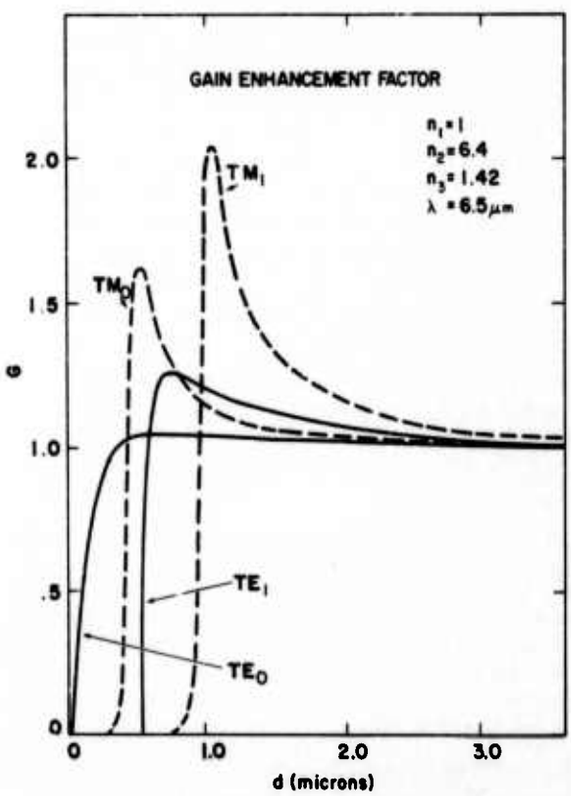

FIG. 6. Gain enhancement factor defined in Eq. (17) vs the film thickness for the first two TE and TM modes.

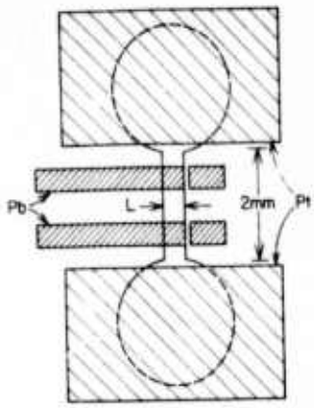

FIG. 7. Schematic drawing showing a completed sample. Since each Pb strip can be biased with either Pt contact, lasing can be obtained in this structure from four different optical cavities.

waves:

$$A\exp[i(\beta x-\omega t)]\cos(k_2 z)=\tfrac{1}{2}A\{\exp[i(\beta x+k_2 z-\omega t)]+\exp[i(\beta x-k_2 z-\omega t)]\}.$$

The power in each plane wave is reduced after a single reflection by the factor $\exp[-(4\pi n_2\sigma\cos\theta_2/\lambda)^2]$, where σ is the variance of the surface height, assumed to be the same for both surfaces, $\theta_2=\arctan(\beta/k_2)$ is the angle of incidence measured from the normal, and λ is the free-space wavelength. Using this method, one can show that the power attenuation coefficient α_s for both TE and TM modes can be written in the form

$$\alpha_s=\left(\frac{4\pi n_2\sigma}{\lambda}\right)^2\frac{\cos^3\theta_2}{\sin\theta_2}\frac{1}{d_{eff}}, \tag{12}$$

where d_{eff} is given by

$$d_{eff,TE}=d+k_1^{-1}+k_3^{-1},$$
$$d_{eff,TM}=d+\frac{n_1^2n_2^2}{k_1}\frac{k_1^2+k_2^2}{n_1^4k_2^2+n_2^4k_1^2}+\frac{n_2^2n_3^2}{k_3}\frac{k_2^2+k_3^2}{n_3^4k_2^2+n_2^4k_3^2}. \tag{13}$$

The quantity d_{eff} describes the effective spatial extent of a mode in the z direction. The expressions (13) are derived by considering the power flow. For a mode far away from cutoff, d_{eff} will nearly equal d. As a mode approaches cutoff, however, d_{eff} rapidly diverges.

We show in Fig. 5 the surface scattering loss coefficients as a function of film thickness calculated from Eqs. (12) and (13). Ignoring the sharp drops in the losses at cutoff, the TE_0 mode shows the lowest loss for all d values of interest.

D. Gain enhancement

Optical gain in a semiconductor is obtained by population inversion induced through minority-carrier injection. This population inversion contributes a small negative imaginary component $\delta\epsilon$ to the dielectric constant. The gain coefficient for plane waves α_p resulting from $\delta\epsilon$ is given by

$$\alpha_p=(k/n_2)\delta\epsilon. \tag{14}$$

In a waveguide, the gain coefficient for a mode will differ from the plane-wave result for two reasons: (i) The guided mode can be viewed as taking a zigzag path down the film. This will increase the effective path length and thus will increase the gain coefficient. (ii) The guided mode has evanescent tails extending into the surrounding passive media. This mode leakage effect will tend to decrease the gain.

To calculate the gain coefficient, we observe that Eq. (1) is identical in form to the one-dimensional Schroedinger equation for a particle in a square well.[16] This means we can use first-order perturbation theory to calculate the change in the eigenvalue β^2 caused by a small change in the index. The result for TE modes is

$$\delta(\beta^2)=\left(\int_{-\infty}^{\infty}|E_y^2|\,\delta\epsilon(\omega^2/c^2)\,dz\right)\left(\int_{-\infty}^{\infty}|E_y^2|\,dz\right)^{-1}. \tag{15}$$

Since the minority-carrier diffusion length is typically an order of magnitude larger than the film thickness, we can assume that $\delta\epsilon$ is uniform across the guide. With this simplification we can write the gain enhancement factor G, defined to be the gain coefficient for the mode α divided by that for a plane wave, in the following form:

$$G=\alpha/\alpha_p=(n_2k/\beta)\left(\int_{-z_{23}}^{z_{12}}|E_y^2|\,dz\right)\left(\int_{-\infty}^{\infty}|E_y^2|\,dz\right)^{-1}. \tag{16}$$

A slightly more complicated expression applies for TM modes. The first factor in Eq. (16) is always less than unity.

Evaluating the integrals in Eq. (16) leads to the following expressions for G:

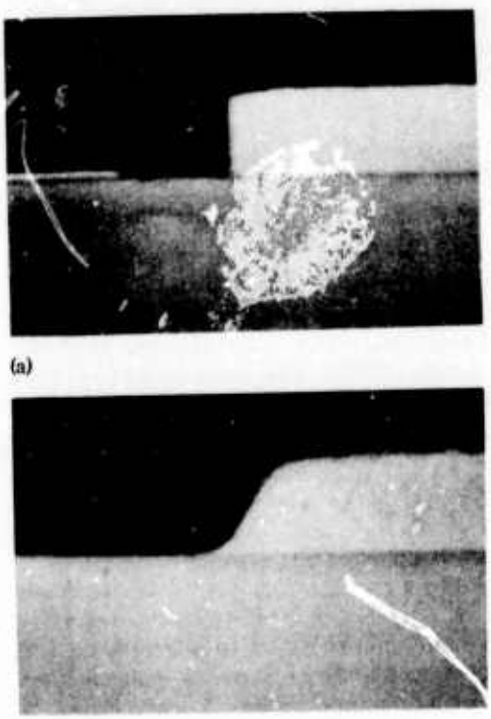

FIG. 8. Scanning electron microscope photographs of two laser end reflectors. The samples have been potted in epoxy and lapped edgewise. In (a) the edge is defined by the photoresist technique. The light streak at the left-hand side is the Pb film. In (b) the edge is defined by a close-spaced evaporation mask.

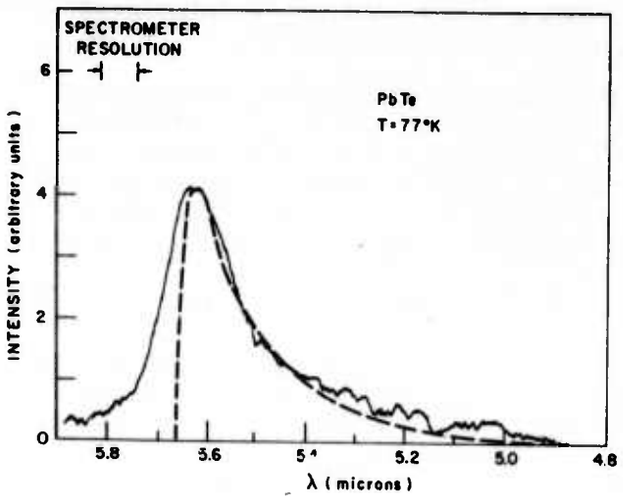

FIG. 9. Spontaneous emission spectrum at 77°K. The dashed line is calculated from Eq. (21) with the peak rounded to indicate some residual attenuation. Device parameters: $p = 1.5 \times 10^{17}$ cm^{-3}, $d = 4.6$ μm, $L = 400$ μm.

$$G_{TE} = \frac{n_2 k}{\beta}\left(d + \frac{k_1}{k_1^2 + k_2^2} + \frac{k_3}{k_3^2 + k_2^2}\right)(d_{eff,TE})^{-1}$$

$$G_{TM} = \frac{n_2 k}{\beta}\left(d + \left(\frac{n_2^2 n_1^2 k_1}{n_2^4 k_1^2 + n_1^4 k_2^2} + \frac{n_2^2 n_3^2 k_3}{n_2^4 k_3^2 + n_3^4 k_2^2}\right)\frac{\beta^2 - k_2^2}{n_2^2 k^2}\right)(d_{eff,TM})^{-1}. \quad (17)$$

These expressions are plotted in Fig. 6 for the first two modes. Note that the TM modes show substantially more gain enhancement than the TE modes. This results from the stronger optical confinement associated with the TM modes.

III. EXPERIMENTAL

A. Sample preparation

PbTe films are grown epitaxially on cleaved (111) BaF_2 substrates. The details of this growth technique and the characterization of the films have been described previously.[8] Hall effect measurements are used to determine the carrier concentrations and mobilities. The as-grown films are p-type with $p = 6 \times 10^{16} - 4 \times 10^{17}$ cm^{-3}. Typical mobilities at 10°K are $(2-5) \times 10^4$ cm^2/V sec, and typical film thicknesses are 2–4 μm.

Since it is not possible to produce cleaved end faces on the thin films, as is normally done with bulk devices, we have developed a photoresist etching technique to produce Fabry-Perot cavities with nearly square ends. The laser cavity is formed by first depositing a dumbbell-shaped mask on the PbTe film with Shipley AZ-111 photoresist. The exposed PbTe is etched away with an HBr : Br = 10 : 1 solution in an equal volume of water. The photoresist is then removed and a ~4000 Å Pt film is sputtered onto the ends of the dumbbell to form the Ohmic contacts. Finally, ~2000 Å Pb strips 150–400 μm wide are evaporated across the PbTe to form the Schottky barriers. The Pb is evaporated at an angle of 45° with respect to the film normal. This procedure serves two purposes. It gives a better electrical connection across the sharp edge of the film on one side, and it leaves the other side bare, permitting the light to exit. A schematic drawing of a completed sample is shown in Fig. 7.

The samples are mounted with a thermal conducting epoxy on copper plates connected directly to the cold finger of a liquid-helium Dewar. The plates are positioned with the dumbbell vertical, and the light emitted within a cone of half-angle 17° centered roughly 20° from the plane of the substrate is collected and focused onto the entrance slit of a grating spectrometer. This sample orientation provides maximum light collection efficiency. The light at the exit slit is focused onto a Ge:Au liquid-nitrogen-cooled photoconductor. For pulsed operation, the current pulses are 2 μsec long at a repetition rate of a few kHz, and boxcar integration is used. For cw operation, the light at the entrance slit is mechanically chopped at 330 Hz and synchronous detection is used.

The importance of using an etching technique to define the laser end reflectors is demonstrated in Fig. 8. Here we show scanning electron microscope photographs of the cross sections of two laser ends—one prepared as described above, the other defined by a close-spaced evaporation mask. The guide end for the etched sample is normal to the substrate to within the accuracy that we can measure it. For the other sample, however, the guide end deviates from normal by an angle $\nu \tilde{=} 0.5$ rad, which would lead to a power reflectivity for a zero-order mode several orders of magnitude below that for an ideal end reflector.

Normally a Schottky barrier diode is a majority-carrier device leading to the recombination of majority carriers at the metal surface with little or no light emission. A Pb film on p-type PbTe, however, produces an n-type inversion layer which can lead to electron injection. Nill *et al.* have shown that under high forward bias this structure is apparently as efficient at injecting minority carriers as a normal p-n junction.[17,18] This result is consistent with our estimates of the internal quantum efficiency η for spontaneous emission at low temperature.[10] We find in our devices a value for η of about 1%, while the best bulk p-n junction yield values in the range 1–5%.

B. Spontaneous emission at 77°K

Previous measurements of both photoluminescence[19] and electroluminescence[10] in PbTe indicate that the emission arises from direct band-to-band recombination with k conservation; i.e., only near-vertical transitions are allowed. The primary evidence for this interpretation from our data is the observation of a highly asymmetric line shape with a sharp cutoff at the band gap on the low-energy side of the peak and a long tail on the high-energy side. The impurity-banding non-k-conservation model of Lasher and Stern[20] has been used to interpret emission from PbSe.[21] However, this model predicts a more symmetric line shape with a substantial tail extending to energies less than the band gap, which does not give a good fit to our data. We will thus restrict our discussion to the k-conservation model. For PbTe this model yields the following expression for the total spontaneous emission rate as a function of the

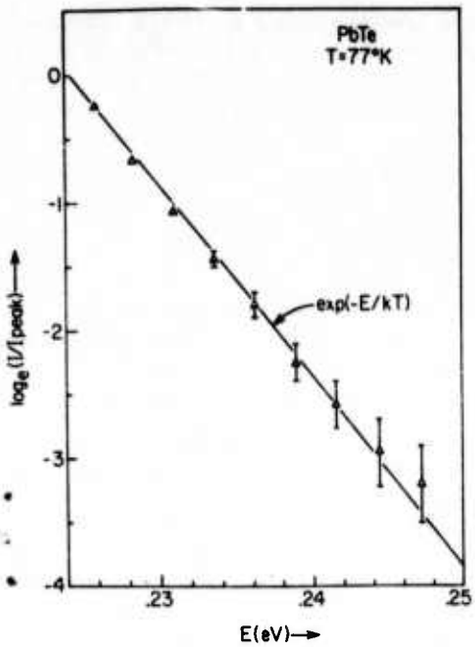

FIG. 10. Semilog plot of the spontaneous emission spectrum on the high-energy side of the peak. The solid line is the slope predicted by Eq. (21). Device parameters: $p = 4.8 \times 10^{17}$, $d = 4.8\ \mu$m, $L = 400\ \mu$m.

energy E[20,22]:

$$r_{sp}(E) = A(E - E_G)^{1/2} f_c(\tfrac{1}{2}E - \tfrac{1}{2}E_G + E_c) \times [1 - f_v(\tfrac{1}{2}E_G - \tfrac{1}{2}E + E_v)], \quad (18)$$

where

$$A = \frac{4n_2 e^2 E E_G m_d^{1/2}(m_d + m_0)}{m_0 \hbar^5 c^3 \pi^2};$$

$m_d = 0.052\ m_0$ is the density-of-states effective mass,[23] which is taken to be the same for both bands; E_c and E_v are the conduction and valence band edges, respectively; $E_G = E_c - E_v$ is the band gap; m_0 is the free-electron mass; f_c and f_v are the Fermi occupation probabilities for electrons in the conduction and valence bands, respectively, given by

$$f_c(E) = \{1 + \exp[(E - \mu_c)/kT]\}^{-1}$$
$$f_v(E) = \{1 + \exp[(E - \mu_v)/kT]\}^{-1}; \quad (19)$$

and μ_c, μ_v are the respective quasi-Fermi levels of the conduction and valence bands. The dimensions of $r_{sp}(E)$ are eV^{-1} cm^{-3} sec^{-1}.

The experimentally observed spectrum $I(E)$ will be modified by reabsorption. The emission from each increment of volume a distance x from the exit face is attenuated by the factor $\exp(-\alpha x)$, where α is the attenuation coefficient. Integrating over x leads to a line shape $r_{sp}(E)/\alpha(E)$. However, $r_{sp}(E)$ and $\alpha(E)$ are related by[20]

$$\alpha(E) = \frac{\pi^2 c^2 \hbar^3}{n_2^2 E^2}\left[\exp\left(\frac{E - \mu_c + \mu_v}{kT}\right) - 1\right] r_{sp}(E). \quad (20)$$

At 77 °K for the range of carrier concentrations and injection levels we are considering, we find that the factor of 1 in Eq. (20) can be neglected compared with the exponential. Thus, for our experimental conditions, the line shape is dominated by a simple Boltzmann factor

$$I(E) \propto \exp(-E/kT). \quad (21)$$

Eqs. (18) and (20) predict a vertical drop in the intensity from its maximum at the band edge. Actually, this corner will be slightly rounded owing to the residual attenuation, such as free-carrier absorption, which does not vanish at this energy.

We show in Fig. 9 an emission spectrum at 77 °K along with the predicted curve. A better way of presenting the data is shown in Fig. 10 for a different sample where we plot $\ln(I/I_{peak})$ vs E above the peak. In both cases, the agreement with Eq. (21) is good. Although the samples used for these data have carrier concentrations differing by a factor of 3, the emission line shapes are essentially the same. In order to observe a change in the linewidth with carrier concentration as was done in the photoluminescence experiments,[18] it is necessary to use higher carrier concentrations and higher injection levels.

It is important to note that the line shape predicted by Eq. (21) in no way depends on the band parameters or carrier concentrations. In fact it does not distinguish electron from hole recombination. In a previous paper, however, we presented data with the light collected through the BaF_2 substrate normal to the film.[10] For that case the reabsorption correction is very small since the light has, on the average, a very short path length through the film. The emission spectrum is broader than it is here, and Eq. (18) with the appropriate effective mass and carrier concentration must be used to fit the data.

Polarization measurements of the spontaneous emission indicate that both polarizations have identical line shapes with the TE intensity (E in the plane of the substrate) being about a factor of 2 larger than the TM intensity. We have not been able to obtain good spontaneous emission spectra at liquid-helium temperatures. Generally, the spectra begin to show stimulated line narrowing at about the same current levels that produce measurable signals through the spectrometer with sufficient resolution.

C. Laser emission at 10–15 °K

Lasing was first observed in these films under pulsed conditions at 12 °K with a threshold current of several hundred millamperes for a typical device—a typical device being 400 μm wide and 4 μm thick with $p \approx 10^{17}$ cm^{-3}. Our best diodes now lase with a threshold current of a few tens of milliamperes. The primary improvement we have made is the use of the photoresist etching technique to define the laser cavity. We have also done some preliminary studies which indicate that the laser performance can be improved by postgrowth annealing at ~350 °C in a Te atmosphere, which increases the carrier concentration to the high 10^{17} or low 10^{18} range. Besides increasing the carrier concentration and mobility, the annealing apparently improves the quantum efficiency.

An example of the cw laser emission from one of our annealed samples is shown in Fig. 11. This device is 2.4 μm thick with a cavity length $L = 400\ \mu$m. The

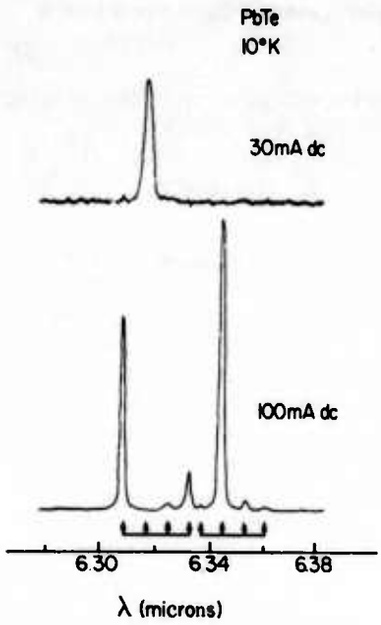

FIG. 11. Laser emission at 10°K for an annealed sample. The upper trace is near the laser threshold. The linewidths in each case are spectrometer resolution limited. The lower trace has twice the resolution, and the signal level is 40× larger than in the upper trace. Each set of four arrows is drawn with an 80-Å spacing. The peak in the upper trace coincides with the second arrow from the left-hand side. Device parameters: $p \approx 10^{18}$ cm^{-3}, $d = 2.4$ μm, $L = 400$ μm.

laser threshold is about 30 mA, corresponding to the upper trace in Fig. 11. The widths of all the lines in the figure are spectrometer resolution limited. The 100-mA trace shows a complicated mode spectrum with seven discernible modes. The four at longer wavelengths show a common mode spacing of ~80 Å. The three remaining modes do not appear to show a common spacing. However, if we insert the 30-mA peak position into the mode pattern at 100 mA, then we again have a set of four modes with an 80-Å spacing as indicated by the arrows in Fig. 11.

Using the mode spacing formula for a plane-wave Fabry-Perot cavity, the effective refractive index $n_{eff} = n - \lambda(dn/d\lambda)$, corresponding to the data in Fig. 11, would be 6.3. Actually, the different waveguide modes will have different effective indices, and we should take this into account. The mode effective indices will always be less than the film effective index. Thus, the use of the plane-wave Fabry-Perot formula will underestimate n_{eff} for the film. For example, if we assume a TE_0 mode for the data in Fig. 11, then n_{eff} would be 6.4 instead of 6.3. We have observed effective indices in some films as large as 8. Such a wide spread in this quantity is not surprising, however, if one considers the large dispersion in $n_2(\lambda)$ near the band edge in PbTe reported by Zemel *et al.*[24] at low temperatures.

The observation of two or three separate sets of Fabry-Perot spaced modes occurs in most devices at currents well above threshold. The reason for this is not clear. It could be due to inhomogenities in the film or on the surface which produce laser filaments in the transverse direction.

All of the laser lines shown in Fig. 11 are polarized ~100% (±5%) with the electric vector in the plane of the substrate, indicating pure TE modes. In fact, we have measured the polarization of 30—40 modes in several different diodes and have invariably found them to be TE polarized, although occasionally the polarization is only 60—80% TE. The observation of modes which are only partially polarized may be another indication of filamentation, since any strong confinement in the direction along the film will lead to modes with mixed TEM polarization. The only cavity property that strongly favors TE modes is the surface scattering loss; thus our results would suggest that this loss mechanism is the dominant one in establishing the laser threshold.

In most samples we observe two prominent laser lines with a separation that is large compared with the cavity mode spacing. This feature usually occurs well above threshold and often only under pulsed conditions. One example is shown by the separation between the two dominant modes in the lower trace in Fig. 11. Another example is shown in Fig. 12 for a different sample. The small splitting of the longer-wavelength modes in this figure is the cavity mode spacing. We have interpreted the large splitting as arising from a strain-induced shift of the energy bands.

The thermal expansion coefficient of the substrate is less than that of the film. This means that at low temperatures the film will appear stretched in the plane of the substrate, the (111) plane, and compressed in the direction normal to it. This deformation will partially remove the degeneracy of the various conduction and valence bands. Since the band gap in the Pb salts is at the zone boundary in the [111] direction, the bands which are oriented along [111] will shift differently from those along $[11\bar{1}]$, $[1\bar{1}1]$, and $[\bar{1}11]$, which remain degenerate.

To estimate the difference between the band gap at (111) and that at the other three points, we will assume the deformation of the crystal to be equivalent to that produced by a stress S applied uniformly in the directions parallel to the (111) plane. For this stress configuration, the strain tensor ϵ'_{ij} in the coordinate system with the z' axis in the [111] direction will be diagonal with nonzero components: $\epsilon'_{11} = \epsilon'_{22} = (s'_{11} + s'_{12})S$ and $\epsilon'_{33} = 2s'_{31}S$, where s'_{ij} are the elastic compliance constants in the primed coordinate system. This description is, of course, not exact since the actual strain will vary over the thickness of the film. In a thin film, however, we can consider the strain values to be averaged over the thickness. Once the strain tensor is known, the shift of any band edge can be determined by $\Delta E = D_{ij}\epsilon_{ij}$, where the D_{ij} are the appropriate components of the deformation potential tensor.[25] After transforming ϵ'_{ij} into the coordinate system with the cubic crystal axes and using the expressions for D_{ij} given by McMullin,[26] we find that the difference between the two band gaps in PbTe can be written in the form

$$\Delta E_G = \frac{8\epsilon'_{33}(\beta_c - \beta_v)}{1 - 2c_{44}/(c_{11} + 2c_{12})} \approx 6.4\epsilon'_{33}\ (\text{eV}), \qquad (22)$$

where ϵ'_{33} is the strain in the [111] direction, β_c and β_v are the off-diagonal elements of the deformation potential tensor for the conduction and valence bands, re-

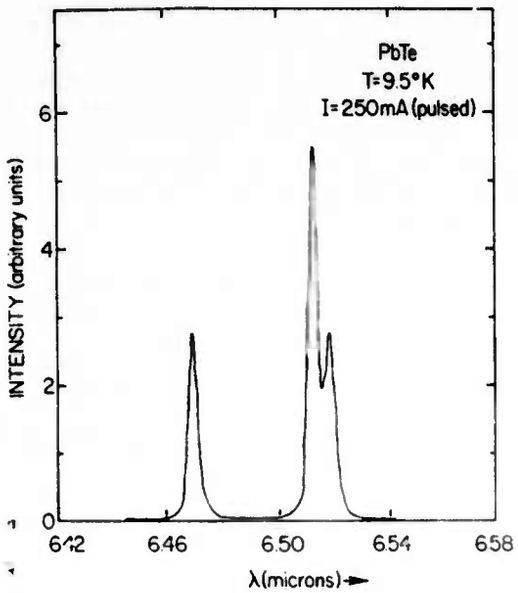

FIG. 12. Pulsed laser emission at 9.5°K in an unannealed sample. The large splitting is roughly 1.4 meV. Device parameters: $p = 1.6\times10^{17}$ cm^{-3}, $d = 2.4$ μm, $L = 400$ μm.

spectively, and the c_{ij} are the standard elastic stiffness constants. We have used the numerical values for these constants summarized in Ref. 26. Our experimental value of the energy gap difference is $\Delta E_G = 1.4$ meV ± 30%, corresponding to a strain $\epsilon'_{33} \approx -2.2\times10^{-4}$.

Recently, Hohnke has measured the temperature dependence of the strain component ϵ'_{33} for similarly grown PbSe films on BaF_2 substrates.[27] He finds that at 77°K $\epsilon'_{33} \approx -3.3\times10^{-4} \pm 10\%$, which is fairly close to the value we would predict from the emission spectra for PbTe. This result is not surprising, however. Since the thermal expansion coefficients for PbTe and PbSe are nearly equal, we would expect the low-temperature strains in the two materials to be similar.

IV. THRESHOLD ANALYSIS AND DISCUSSION

In this section, we present an analysis of the gain and loss parameters which characterize the laser threshold. The analysis will necessarily be very crude since we have no way of independently measuring the various contributions separately. The threshold condition we can write in the form

$$-G\alpha(E_m) = G\alpha_{fc} + \alpha_s + L^{-1}\ln R^{-1}\,, \tag{23}$$

where α_{fc} is the free-carrier absorption, α_s is the surface scattering loss, G is the gain enhancement factor, L is the cavity length, R is the power reflectivity, and $\alpha(E_m)$ is the maximum plane-wave gain coefficient given by Eqs. (18) and (20). Under lasing conditions $\alpha(E_m)$ will, of course, be negative. The free-carrier and reflection losses can be estimated reasonably well, but the surface scattering loss α_s involves an unknown scaling parameter, the variance of the surface height. On the other hand, the maximum gain coefficient $\alpha(E_m)$ can be related to the threshold current in the diode by

$$I_t = (eV/\eta)\int r_{sp}(E)\,dE, \tag{24}$$

where I_t is the threshold current, V is the recombination volume, and η the internal quantum efficiency. Thus, the least-known parameter in Eq. (23) is the surface scattering loss, and our aim will be to use estimates of the other quantities to determine it.

Normally Eq. (24) is written with the current density j on the left-hand side and the minority-carrier diffusion length on the right-hand side. That way of expressing the j-vs-$\alpha(E_m)$ relation is appropriate for a bulk p-n junction with the current flow uniformly and normal to the junction plane. In our diodes the current flow is nonuniform with components both normal and transverse to the junction plane. To make the problem tractable, we will make two simplifying assumptions: First, we assume that electron injection occurs predominantly at the edge of the Pb film. This should be a good approximation at high injection when the junction voltage is large compared with kT/e, since the voltage drop along the film will substantially reduce the injection away from the Pb edge nearest the Pt contact. Second, we assume that the electron distribution is uniform in the z and x directions and spread out by the diffusion length in the y direction. This should be a good approximation at low temperatures where the minority-carrier diffusion length L_n is roughly an order of magnitude greater than the film thickness. Our entire analysis of the waveguiding properties implicitly assumes that lasing begins not in the region covered by the Pb film, but in the region adjacent to it. This will certainly be the case near threshold where the additional losses of the metal film would preclude lasing in that region. Thus the recombination volume V is a rectangular region with thickness d, width L_n, and length L. The accepted value for the minority-carrier diffusion length in Pb-salt lasers is roughly 20 μm,[5,6] but we will take $L_n = 40$ μm since the carriers can diffuse in both the plus and minus y directions.

In the spirit of our approximate treatment we will use a simplified expression for estimating the optical gain at threshold rather than the integral relation (24). This simple expression can be written in the form[22]

$$-\alpha(E_m) = I_t\eta\pi^2c^2\hbar^3/eVn_2^2\gamma E_m^2\Delta E\,, \tag{25}$$

where γ is the "demerit" factor and ΔE is a measure of the spontaneous linewidth. We have found that using $\gamma\Delta E = 4.3$ meV in Eq. (25) leads to a value which is always within about 20% of the value calculated from Eq. (24) for a particular threshold condition. The quantum efficiency was measured previously to be about 1% for unannealed samples.[10]

In Table I we show typical threshold data for four PbTe lasers. The threshold current is determined by examing both the emission spectrum and the variation

TABLE I. Threshold characteristics for thin-film PbTe diode lasers.

Sample	Film thickness (μm)	Cavity length (μm)	Threshold current (A)	$-\alpha(E_m)$ (cm^{-1})	α_{fc} (cm^{-1})	$L^{-1}\ln R^{-1}$ (cm^{-1})	α_s (cm^{-1})	σ (μm)
242-3b	4.5	400	0.17	59	6.2	12	41	0.052
272-1a	3.2	400	0.41	200	1.2	10	189	0.059
299-3d	2.8	400	0.18	100	1	9.6	90	0.032
307-3a	2.4	180	0.13	188	1.3	20	167	0.033

of the light intensity with current. The uncertainty in this determination is about 10%. The optical gain is calculated from Eq. (25) with $\eta = 1\%$ and $\gamma\Delta E = 4.3$ meV. The free-carrier absorption coefficient is calculated from[28]

$$\alpha_{fc} = \frac{pe^3\lambda^2}{4\pi^3 n_2 c^3 \epsilon_0 \mu_p m_c^2}, \tag{26}$$

where $m_c = 0.032 m_0$ is the conductivity effective mass[29]; p and μ_p are the hole carrier concentration and mobility, respectively, which are measured for each device, and ϵ_0 is the free-space dielectric constant. The reflection loss is determined from Fig. 3 by assuming a TE_0 mode. The surface scattering loss is determined from the threshold condition (25) by using a gain enhancement factor of unity. The value of σ is calculated from Fig. 5, again by assuming a TE_0 mode. In every case α_s is the dominant loss contribution. This is consistent with the observed strong preference for TE modes. The values for σ given in Table I should be considered as upper limits since we have probably overestimated the carrier confinement by the assumption of a line source of injection and there may indeed be other losses which we have overlooked. In the absence of an experimental verification of the surface loss theory and its applicability to our films, it is more appropriate to view σ as a phenomenological parameter characterizing the surface loss, rather than a true measure of the variance of the surface height.

Annealed samples show a factor of 3–5 lower threshold current densities than unannealed ones. Presumably this results from an increase in η, in which case the predicted values of σ for those samples would again be the same magnitude as those shown in Table I. Annealing also produces a shift of about 2% of the laser emission to higher energies. An example of this shift can be seen by comparing Figs. 11 and 12. The shift arises from the increase in carrier concentration. With higher hole concentrations, higher energy transitions are allowed. These transitions involve a larger density of states than those closer to the band edges and thus will tend to be favored for lasing.

The primary conclusion we can draw from this threshold analysis is that there are large losses in addition to free-carrier and reflection losses which are important in determining the laser threshold. Significant improvements in the laser performance can be expected if these losses are reduced. Coupled with the increased quantum efficiency from annealing, laser thresholds as low as 1 mA should be attainable in our devices. In addition a high-gain single-pass optical amplifier could be made by eliminating the end reflectors and adding input and output grating couplers at the ends of the active region.

ACKNOWLEDGMENTS

The authors are indebted to H. Holloway, E. M. Logothetis, and A. J. Varga for participating in the development of the device fabrication techniques which made this research possible. They would also like to thank D. K. Hohnke, P. V. S. Rao, and S. W. Kaiser for providing them with samples and with expert technical advice regarding the annealing, etching, and other device preparation procedures, M. Mikkor for the excellent electron microscope photographs, Professor G. W. Ford for several discussions regarding the mode reflectivity calculations, and S. L. McCarthy for a critical reading of the manuscript.

*Research supported in part by The Advanced Research Projects Agency of the Department of Defense and was monitored by ORN under Contract No. N00014-73 C-0289.

[1] J. F. Butler, A. R. Calawa, R. J. Phelan, Jr., T. C. Harman, A. J. Strauss, and R. H. Rediker, Appl. Phys. Lett. 5, 75 (1964).
[2] J. F. Butler, A. R. Calawa, R. J. Phelan, Jr. A. J. Strauss, and R. H. Rediker, Solid State Commun. 2, 303 (1964).
[3] J. F. Butler and A. R. Calawa, J. Electrochem. Soc. 112, 1056 (1965).
[4] J. F. Butler, A. R. Calawa, and T. C. Harman, Apply. Lett. 9, 427 (1966).
[5] T. C. Harman, in *The Physics of Semimetals and Narrow-Gap Semiconductors*, edited by D. L. Carter and R. T. Bate (Pergamon, Oxford, England, 1971), p. 363.
[8] R. W. Ralston, I. Melngallis, A. R. Calawa, and W. T. Lindley, IEEE J. Quantum Electron, QE-9, 350 (1973).
[7] P. Zoutendyk, Ph. D. thesis (California Institute of Technology, 1968) (unpublished).
[8] H. Holloway, J Nonmetals (to be published); other references to the materials growth can be found in this paper.
[9] E. M. Logothetis, H. Holloway, A. J. Varga, and E. Wilkes, Appl. Phys. Lett. 19, 318 (1971).
[10] H. Holloway, W. H. Weber, E. M. Logothetis, A. J. Varga, and K. F. Yeung, Appl. Phys. Lett. 21, 5 (1972).
[11] P. K. Tien, Appl. Opt. 10, 2395 (1971).
[12] D. H. Hensler, J. D. Cuthbert, R. J. Martin, and P. K. Tien, Appl. Opt. 10, 1937 (1971).
[13] F. K. Reinhart, I. Hayashi, and M. B. Panish, J. Appl. Phys. 42, 4466 (1971).
[14] D. F. Nelson and J. McKenna, J. Appl. Phys. 38, 4057 (1967).
[15] P. Beckmann and A. Spizzichino, *The Scattering of Electromagnetic Waves from Rough Surfaces* (Pergamon, Oxford, England, 1963).
[16] K. O. Hill, A. Watanabe, and J. G. Chambers, Appl. Opt. 11, 1952 (1972).
[17] K. W. Nill, A. R. Calawa, T. C. Harman, J. N. Walpole, Appl. Phys. Lett. 16, 375 (1970).
[18] K. W. Nill, J. N. Walpole, A. R. Calawa, and T. C. Harman, in *The Physics of Semimetals and Narrow-Gap Semiconductors*, edited by D. L. Carter and R. T. Bate (Pergamon, Oxford, England. 1971), p. 383.
[19] E. R. Washwell and F. F. Cuff, *Radiative Recombination Symposium, Paris* (Academic, New York, 1964), p. 11.
[20] G. Lasher and F. Stern, Phys. Rev. 133, A553 (1964).
[21] J. M. Besson, W. Paul, and A. R. Calawa, Phys. Rev. 173, 699 (1968).
[22] M. J. Adams and P. T. Landsberg, in *Gallium Arsenide Lasers*, edited by C. H. Gooch (Wiley, New York, 1969), Chap. 2.
[23] For a summary of the Pb-salt band parameters see R. Dalven, Infrared Phys. 9, 141 (1969).
[24] J. N. Zemel, J. D. Jensen, and R. B. Schoolar, Phys. Rev. 140, A330 (1965).
[25] L. G. Ferreira, Phys. Rev. 137, A1601 (1965).
[26] P. G. McMullin, PhD. thesis (Massachusetts Institute of Technology, 1971) (unpublished).
[27] D. K. Hohnke (unpublished).
[28] T. S. Moss, *Optical Properties of Semiconductors* (Butterworths, London, 1959), p. 30.
[29] H. A. Lyden, Phys. Rev. 135, A514 (1964).